

# Journal of Mechanics of Materials and Structures

**NONLINEAR FEM ANALYSIS FOR BEAMS  
AND PLATE ASSEMBLAGES BASED  
ON THE IMPLICIT COROTATIONAL METHOD**

Giovanni Garcea, Antonio Madeo and Raffaele Casciaro

**Volume 7, No. 6**

**June 2012**

## NONLINEAR FEM ANALYSIS FOR BEAMS AND PLATE ASSEMBLAGES BASED ON THE IMPLICIT COROTATIONAL METHOD

GIOVANNI GARCEA, ANTONIO MADEO AND RAFFAELE CASCIARO

In our previous paper the implicit corotational method (ICM) was presented as a general procedure for recovering objective nonlinear models fully reusing the information obtained by the corresponding linear theories.

The present work deals with the implementation of the ICM as a numerical tool for the finite element analysis of nonlinear structures using either a path-following or an asymptotic approach. Different aspects of the FEM modeling are discussed in detail, including the numerical handling of finite rotations, interpolation strategies, and equation formats.

Two mixed finite elements are presented, suitable for nonlinear analysis: a three-dimensional beam element, based on interpolation of both the kinematic and static fields, and a rotation-free thin-plate element, based on a biquadratic spline interpolation of the displacement and piece-wise constant interpolation of stress. Both are frame invariant and free from nonlinear locking.

A numerical investigation has been performed, comparing beam and plate solutions in the case of thin-walled beams. The good agreement between the recovered results and the available theoretical solutions and/or numerical benchmarks clearly shows the correctness and robustness of the proposed approach as a general strategy for numerical implementations.

### 1. Introduction

In our previous paper [Garcea et al. 2012] we described a general methodology, called the implicit corotational method (ICM), able to build geometrically exact nonlinear structural models by exploiting the information gained from linear theories. It is essentially based on two main steps: the general solution provided by the linear theory is exploited to recover a description of the nonlinear stress and strain fields, as viewed by a corotational local observer moving with the material neighbor; then this description is transferred to a fixed global frame directly by using standard change-in-the-observer algebra. In this way a general procedure which can be implemented in a simple and automatic way in different contexts is derived. The recovered nonlinear models implicitly satisfy objectivity requirements (they are geometrically exact) and maintain all the details of the three-dimensional linear solutions, without any deterioration.

---

This paper has been developed within the national joint research project “Performance-based modeling and analysis of nonlinear structures,” supported by the Italian Ministry of University Scientific and Technology Research (MIUR). We would like to thank all the participants in the project for their comments and suggestions. Special thanks are addressed to Giuseppe Zagari, for his help in setting up the computer codes and performing the numerical tests.

*Keywords:* geometrically exact beam and shell theories, corotational description, postbuckling analysis.

Since linear structural theories are widely available in the literature, it is easy to obtain a large number of possible nonlinear models suitable for use in FEM analysis. Three ICM models have been derived in [Garcea et al. 2012]: a three-dimensional beam nonlinear model based on Saint-Venant general rod theory and two plate/shell nonlinear models based on Mindlin–Reissner and Kirchhoff plate theories.

In this paper we deal with the FEM implementation and numerical validation of these models within different analysis strategies. We start by discussing, in Section 2, the two analysis contexts which have been investigated, a *path-following analysis*, according to Riks’ incremental iterative strategy [Riks 1979], and an *asymptotic analysis*, according to the Koiter-like approach described in [Casciaro 2005]. The latter, because of its exacting requirements in terms of the geometrical coherence of the modeling, provides a rigorous check on the accuracy obtained with the ICM approach.

The general aspects of ICM implementation in FEM analysis will be examined in Section 2.1. We will also consider different choices in the element description (that is, Lagrangian or corotational description) and in the interpolation of its internal fields. Frame-independence plays an important role in element setup and the lack of it can result in spurious locking, which we called nonlinear interpolation locking in [Casciaro 2005] (also see [Salerno and Lanzo 1997]), which can significantly affect the numerical solution. The equation format (that is, mixed or compatible) also plays an important role in the convergence of the iterative solution processes and in the accuracy of the extrapolation results (see [Garcea et al. 1998; 1999]). These topics will be discussed and the use of mixed FEM interpolations and a mixed format is suggested.

Sections 4 and 5 will present and describe in detail two finite elements derived by the beam and Kirchhoff plate ICM models recovered in [Garcea et al. 2012], which appear suitable for the analysis of general three-dimensional assemblages. Both use a mixed format and a separate interpolation of the displacement and stress fields and are free from interpolation nonlinear locking. The beam element represents a three-dimensional extension of the interpolation described in [Salerno and Lanzo 1997]; the plate element is based on the biquadratic spline interpolation already used in [Lanzo et al. 1995; Lanzo and Garcea 1996; Casciaro et al. 1998; Garcea 2001]

The availability of analytical results or known reference benchmarks and the possibility of comparing, in the case of thin-walled beams, the results obtained by two different models (such as a one-dimensional beam or an assemblage of two-dimensional plates) allow, in Section 6, a detailed discussion about the performance of the proposed elements and their effectiveness in test cases of technical interest. Final comments and remarks are made in the concluding section.

## 2. Numerical strategies in nonlinear FEM analysis

In reviews of the numerical strategies used in nonlinear FEM analysis, Riks [1987; 2004] identified two main approaches: the *path-following* and *asymptotic* analyses. Both apply to a structure subjected to an assigned loading path  $p[\lambda]$ , usually in the form of a proportional loading  $p := \lambda \hat{p}$ , which is described by defining its potential energy in terms of a discrete set of parameters, all collected into a *configuration vector*  $\mathbf{u}$ , which controls both displacement and stress fields,  $d$  and  $\sigma$ , through the assumed FEM interpolation. According to [Garcea et al. 2012, Equations (1)–(4)], equilibrium implies the condition

$$\Pi' \delta u := \Phi'[u] \delta u - \lambda \hat{p} \delta u = 0, \quad u \in \mathcal{U}, \quad \delta u \in \mathcal{T}, \quad (1)$$

where  $\mathbf{u} := \{d, \sigma\}$ ,  $\Phi[\mathbf{u}]$  is the strain energy,  $\lambda \hat{\mathbf{p}} \mathbf{u}$  the external work, and we denote by a prime Frechét's differentiation. Applying FEM interpolation  $\mathbf{u} := \mathcal{L}\mathbf{u}$ ,  $\mathcal{L}$  being the *interpolation operator*, (1) can be rewritten in the vectorial form

$$\mathbf{r}[\mathbf{u}, \lambda] := \mathbf{s}[\mathbf{u}] - \lambda \hat{\mathbf{p}} = \mathbf{0}, \quad (2)$$

with the *response vector*  $\mathbf{s}[\mathbf{u}]$  and the *unitary load vector*  $\hat{\mathbf{p}}$  being defined by the energy equivalencies

$$\mathbf{s}^T \delta \mathbf{u} = \Phi'[\mathbf{u}] \delta \mathbf{u}, \quad \hat{\mathbf{p}}^T \delta \mathbf{u} = \hat{\mathbf{p}} \delta \mathbf{u}, \quad \forall \delta \mathbf{u}. \quad (3)$$

We obtain a relationship between the configuration vector  $\mathbf{u}$  and the load multiplier  $\lambda$  defining a curve (maybe composed of several separate branches) in  $\{\mathbf{u}, \lambda\}$  space, usually called the *equilibrium path*. The aim of the analysis will be to obtain an accurate evaluation of its natural branch, that is, the branch coming from a known initial configuration  $\mathbf{u}_0$ , usually assumed as the one corresponding to  $\lambda = 0$ .

For reading convenience, we briefly summarize both the cited approaches here and refer interested readers to the specific literature for further details (for example, see [Riks 2004; Casciaro 2005] and references therein).

**2.1. Path-following analysis.** The basic idea in this approach is to recover the equilibrium path by determining a sequence of equilibrium points  $\{\mathbf{u}^{(k)}, \lambda^{(k)}\}$  sufficiently near to allow the equilibrium curve to be obtained by interpolation. The analysis develops into a step-by-step process. In each step, a new point  $\{\mathbf{u}^{(k+1)}, \lambda^{(k+1)}\}$  is determined, starting from a first evaluation  $\{\mathbf{u}_1, \lambda_1\}$  generally obtained by an extrapolation of the previous step, by an iterative Newton-like scheme which provides a convergent sequence of estimates  $\{\mathbf{u}_j, \lambda_j\}$ ,  $j = 2, 3, \dots$ , so allowing us to reduce the equilibrium error  $\mathbf{r}_j := \mathbf{r}[\mathbf{u}_j, \lambda_j]$  to within an acceptable tolerance.

Different schemes have been proposed in the literature to perform the iteration, but all of them appear as minor variations of the *arc-length scheme* originally proposed in [Riks 1979]. The main idea is that of coupling the equilibrium equation (2) with the further constraint

$$g[\mathbf{u}, \lambda] - \xi^{(k+1)} = 0, \quad (4a)$$

which defines a surface in  $\{\mathbf{u}, \lambda\}$  space, so the required solution will correspond to the intersection of this surface with the equilibrium curve (2). Different variants of the method are obtained by different choices for the function  $g[\mathbf{u}, \lambda]$ .

The conditions for achieving a proper intersection between (2) and (4a) are extensively described in Riks' papers. The simplest choice, originally suggested by Riks, of using the orthogonal hyperplane

$$\mathbf{n}_u^T (\mathbf{u} - \mathbf{u}_1) + n_\lambda (\lambda - \lambda_1) = 0, \quad (4b)$$

where

$$\mathbf{n}_u := \mathbf{M}(\mathbf{u}_1 - \mathbf{u}^{(k)}), \quad n_\lambda := \mu(\lambda_1 - \lambda^{(k)}), \quad (4c)$$

$\mathbf{M}$  and  $\mu$  being some suitable metric factors, will be effective (see [Garcea et al. 2002] for a discussion of this topic).

Solution of the extended system (2)–(4b) can be obtained by a modified Newton–Raphson scheme:

$$\mathbf{u}_{j+1} = \mathbf{u}_j + \dot{\mathbf{u}}, \quad \lambda_{j+1} = \lambda_j + \dot{\lambda}, \quad (5a)$$

where by introducing matrix  $\tilde{\mathbf{K}}$  as a suitable approximation for the Hessian of the strain energy  $\Phi[\mathbf{u}]$ :

$$\tilde{\mathbf{K}} \approx \mathbf{K}[\mathbf{u}_j] := \left[ \frac{\partial \mathbf{s}[\mathbf{u}]}{\partial \mathbf{u}} \right]_{\mathbf{u}_j}, \quad (5b)$$

the iterative corrections  $\dot{\mathbf{u}}$  and  $\dot{\lambda}$  are defined by the linear system

$$\begin{bmatrix} \tilde{\mathbf{K}} & \hat{\mathbf{p}} \\ \mathbf{n}_u^T & n_\lambda \end{bmatrix} \begin{bmatrix} \dot{\mathbf{u}} \\ \dot{\lambda} \end{bmatrix} = - \begin{bmatrix} \mathbf{r}_j \\ 0 \end{bmatrix}, \quad (5c)$$

which is easily solved in partitioned form allowing us to exploit the symmetry and banded structure of matrix  $\tilde{\mathbf{K}}$ .

The arc-length scheme provides a simple way to overcome limit points because the extended system (5c) remains not singular even if the Hessian  $\mathbf{K}$  becomes singular, which was a real difficulty before the paper [Riks 1979]. Its behavior is, however, strongly affected by the choice for the iteration matrix  $\tilde{\mathbf{K}}$  which is usually assumed as the Hessian evaluated in correspondence to  $\mathbf{u}^{(k)}$  (that is, at the beginning of the step) or to  $\mathbf{u}_1$  (in the first extrapolation point). The convergence of the iterative process (5) has been widely discussed in [Garcea et al. 1998; Casciaro and Garcea 2002]. It is highly sensitive to the format of the equations, that is to the actual manner in which the equations are split and organized (also see [Garcea and Leonetti 2011; Bilotta et al. 2012]). Different formats behave very differently and, in particular, compatible formats expressed in displacement unknowns and equilibrium equations can lead to convergence failures as a consequence of locking (which we call *extrapolation locking* in [Garcea et al. 1998]) due to the interaction of large axial/flexural stiffness ratios with even small element rotations.

As regards the aim of the present paper, it is important to consider that path-following analysis only needs the response vector  $\mathbf{s}[\mathbf{u}]$ , that is, the first variation of the strain energy, to be evaluated accurately, being directly related to (2). Conversely, the same accuracy is not actually needed for the second variation of the energy which provides the Hessian matrix  $\mathbf{K}[\mathbf{u}]$ , because it is only used as a part of the iteration process and its accuracy only influences the convergence of the process. A fairly rough approximation is generally sufficient for that purpose.

**2.2. The asymptotic analysis.** Asymptotic analysis essentially corresponds to the implementation of Koiter's approach to nonlinear elastic stability [Koiter 1945; Budiansky 1974] into a FEM numerical context. While being less diffuse than path-following approaches within computational mechanics (maybe because of its high demands in terms of modeling accuracy) it has been described in detail in many papers (for example, [Casciaro et al. 1992; 1998; Flores and Godoy 1992; Lanzo et al. 1995; Pacoste and Eriksson 1995; Lanzo and Garcea 1996; Wu and Wang 1997; Poulsen and Damkilde 1998; Garcea et al. 1999; 2002; 2005; Garcea 2001; Boutyour et al. 2004; Casciaro 2005; Silvestre and Camoti 2005; Chen and Virgin 2006; Schafer and Graham-Brady 2006; Rahman and Jansen 2010] and references therein), so it only needs to be briefly summarized here.

The solution process is based on an expansion of the potential energy, in terms of load factor  $\lambda$  and modal amplitudes  $\xi_i$ , which is characterized by fourth-order accuracy. Following [Casciaro 2005], it can be summarized in this way:

- (1) The *fundamental path* is obtained as a linear extrapolation

$$\mathbf{u}^f[\lambda] := \mathbf{u}_0 + \lambda \hat{\mathbf{u}}, \quad (6a)$$

where  $\hat{\mathbf{u}}$  is the initial path tangent, obtained as the solution of the linear vectorial equation

$$\mathbf{K}_0 \hat{\mathbf{u}} = \hat{\mathbf{p}}, \quad \mathbf{K}_0 := \mathbf{K}[\mathbf{u}_0]. \quad (6b)$$

- (2) A cluster of *buckling loads*  $\lambda_i, i = 1, \dots, m$ , and associated *buckling modes*  $\hat{\mathbf{v}}_i$  are obtained along  $\mathbf{u}^f[\lambda]$ , defined by the critical condition

$$\mathbf{K}[\lambda_i] \hat{\mathbf{v}}_i = \mathbf{0}, \quad \mathbf{K}[\lambda] := \mathbf{K}[\mathbf{u}_0 + \lambda \hat{\mathbf{u}}]. \quad (6c)$$

We will denote with  $\mathcal{V} := \{\hat{\mathbf{v}} = \sum_{i=1}^m \xi_i \hat{\mathbf{v}}_i\}$  the subspace spanned by the buckling modes  $\hat{\mathbf{v}}_i$  and with  $\mathcal{W} := \{\mathbf{w} : \mathbf{w} \perp \hat{\mathbf{v}}_i, i = 1, \dots, m\}$  its orthogonal complement according the orthogonality condition

$$\mathbf{w} \perp \hat{\mathbf{v}}_i \Leftrightarrow \Phi_b''' \hat{\mathbf{u}} \hat{\mathbf{v}}_i \mathbf{w} = 0, \quad (6d)$$

where  $\hat{\mathbf{u}} := \mathcal{L} \hat{\mathbf{u}}$ ,  $\hat{\mathbf{v}}_i := \mathcal{L} \hat{\mathbf{v}}_i$ , and  $\mathbf{w} := \mathcal{L} \mathbf{w}$ . We will also denote with  $\lambda_b$  an appropriate reference value for the cluster, for example, the smallest of  $\lambda_i$  or their mean value, and with a suffix ‘‘b’’ quantities evaluated in correspondence to  $\mathbf{u}_b := \mathbf{u}^f[\lambda_b]$ .

- (3) Making  $\xi_0 := (\lambda - \lambda_b)$  and  $\hat{\mathbf{v}}_0 := \hat{\mathbf{u}}$ , for more compact notation, the asymptotic approximation for the required path is defined by the expansion

$$\mathbf{u}[\lambda, \xi_k] := \mathbf{u}_b + \sum_{i=0}^m \xi_i \hat{\mathbf{v}}_i + \frac{1}{2} \sum_{i,j=0}^m \xi_i \xi_j \mathbf{w}_{ij}, \quad (6e)$$

where  $\mathbf{w}_{ij} \in \mathcal{W}$  are quadratic corrections introduced to satisfy the projection of equilibrium equation (1) into  $\mathcal{W}$  and obtained by the linear *orthogonal equations*

$$\delta \mathbf{w}^T (\mathbf{K}_b \mathbf{w}_{ij} + \mathbf{p}_{ij}) = 0, \quad \forall \mathbf{w} \in \mathcal{W}, \quad (6f)$$

where  $\mathbf{K}_b := \mathbf{K}[\mathbf{u}^f[\lambda_b]]$  and vectors  $\mathbf{p}_{ij}$  are defined as a function of modes  $\hat{\mathbf{v}}_i$  and  $i = 0, \dots, m$  by the energy equivalence

$$\delta \mathbf{w}^T \mathbf{p}_{ij} = \Phi_b''' \delta \mathbf{w} \hat{\mathbf{v}}_i \hat{\mathbf{v}}_j.$$

- (4) The following energy terms are computed for  $i, j = 0, \dots, m$  and  $k = 1, \dots, m$ :

$$\begin{aligned} \mathcal{A}_{ijk} &= \Phi_b'' \hat{\mathbf{v}}_i \hat{\mathbf{v}}_j \hat{\mathbf{v}}_k, & \mathcal{B}_{ijhk} &= \Phi_b''' \hat{\mathbf{v}}_i \hat{\mathbf{v}}_j \hat{\mathbf{v}}_h \hat{\mathbf{v}}_k - \Phi_b'' (w_{ij} w_{hk} + w_{ih} w_{jk} + w_{ik} w_{jh}), \\ \mathcal{C}_{ik} &= \Phi_b'' w_{00} w_{ik}, & \mu_k[\lambda] &= \frac{1}{2} \lambda_b (\lambda - \frac{1}{2} \lambda_b) \Phi_b''' \hat{\mathbf{u}}^2 \hat{\mathbf{v}}_k + \frac{1}{6} \lambda_b^2 (\lambda_b - 3\lambda) \Phi_b'''' \hat{\mathbf{u}}^3 \hat{\mathbf{v}}_k, \end{aligned} \quad (6g)$$

where the *implicit imperfection factors*  $\mu_k$  are defined by the fourth-order expansion of the unbalanced work on the fundamental path (that is,  $\mu_k[\lambda] := (\lambda \hat{\mathbf{p}} - \Phi'[\lambda \hat{\mathbf{u}}]) \hat{\mathbf{v}}_k$ ).

- (5) The equilibrium path is obtained by projecting equilibrium equation (1) into  $\mathcal{V}$ . According to (6a)–(6g), we have

$$\frac{1}{2} \sum_{i,j=0}^m \xi_i \xi_j \mathcal{A}_{ijk} + \frac{1}{6} \sum_{i,j,h=0}^m \xi_i \xi_j \xi_h \mathcal{B}_{ijhk} + \mu_k[\lambda] - \lambda_b \left( \lambda - \frac{1}{2} \lambda_b \right) \sum_{i=0}^m \xi_i \mathcal{C}_{ik} = 0, \quad k = 1, \dots, m. \quad (6h)$$

The equation corresponds to an algebraic nonlinear system of  $m$  equations in the  $m + 1$  variables  $\xi_0, \xi_1, \dots, \xi_m$ , with known coefficients.

Note that, from a computational point of view, the analysis develops into:

- (i) Solve linear system (6a); this can easily be obtained by standard factorization of matrix  $\mathbf{K}_0$ .
- (ii) Perform the buckling search (6b); this corresponds to a nonlinear eigenvalue problem which can be, however, easily solved, as described in [Casciaro et al. 1998], by an iterative scheme only requiring matrix  $\mathbf{K}_0^{-1}$  be available in factorized form, as it already is from the previous step.
- (iii) Solve orthogonal equations (6f); they correspond to a linear system where the right-hand vectors  $\mathbf{p}_{ij}$  are obtained as a function of  $\mathbf{v}_i$  by an element-by-element assembling process similar to that used for obtaining  $\mathbf{s}[\mathbf{u}]$ ; as  $\mathbf{K}_b \approx \mathbf{K}_0$  within the orthogonal space  ${}^{\circ}\mathcal{W}$ , its solution can be conveniently obtained, as described in [Casciaro et al. 1998], through a modified Newton-like iteration scheme exploiting  $\mathbf{K}_0$  as an iteration matrix (see [Casciaro 2004] for further insights).
- (iv) Compute factors  $\mathcal{A}_{ijk}, \dots, \mu_k[\lambda]$  through (6g); all of them are scalar quantities which can be easily obtained as integrals of known functions.
- (v) Perform a path-following solution of (6h); because of the small dimensions of the system (of the order of tenths), this can be obtained very quickly using standard or even specialized variants of the arc-length scheme.

The actual implementation of the asymptotic approach as a computational tool is therefore quite easy and its total computational burden, which is mainly involved in the factorization of matrix  $\mathbf{K}_0$ , remains of the order of that required by a standard linearized stability analysis. It provides the initial postbuckling behavior of the structure, including *modal interactions* and *jumping-after-bifurcation* phenomena. Moreover, once the preprocessor phase of the analysis has been performed (Steps (1)–(4)), the presence of small loading imperfections or geometrical defects can be taken into account in the postprocessing phase (Step (5)), by adding some additional imperfection terms in the expression of  $\mu_k[\lambda]$ , with a negligible computational extra cost, so allowing an inexpensive imperfection sensitivity analysis (for example, see [Lanzo and Garcea 1996; Casciaro et al. 1998]). From (6h) we can also extract information about the worst imperfection shapes [Salerno and Casciaro 1997; Salerno and Uva 2006] we can use to improve the imperfection sensitivity analysis or for driving more detailed investigations through specialized path-following analysis (see [Casciaro 2005; Casciaro and Mancusi 2006] and references therein).

Note that asymptotic analysis can provide a very accurate recovery of the equilibrium path, as it derives from both numerical testing and theoretical investigation [Brezzi et al. 1986]. Conversely, it makes great use of information attained from a fourth-order expansion of the strain energy and then requires that a fourth-order accuracy be guaranteed in the structural modeling. Even small inaccuracies in this evaluation, deriving from geometrical incoherencies in the higher-order terms of the expansion of the  $\varepsilon[d]$  law or in its finite element representation, significantly affect the accuracy of the solution and can make it unreliable. It is also very sensitive to the format used in the extrapolation, to avoid *extrapolation locking* (see [Garcea et al. 1999]), and the use of a mixed equation format is generally needed to obtain a robust implementation.

This high sensitivity of the asymptotic analysis to the accuracy in the nonlinear modeling actually represents an advantage for the purposes of the present paper because it provides a very sensitive context and appropriate benchmarks suitable for an in-depth testing of the accuracy of ICM models.

### 3. FEM implementation of nonlinear models

The ICM method [Garcea et al. 2012] allows the recovery of nonlinear models from information attained by the corresponding linear ones. It is particularly suitable for modeling fibred continua, such as beams and shells, and directly provides an objective expression for the mixed form of the potential energy:

$$\Pi := \int_{\Omega} \{ \mathbf{t}[s]^T \boldsymbol{\varrho}[\mathbf{d}[s]] - \frac{1}{2} \mathbf{t}[s]^T \mathbf{H}[s] \mathbf{t}[s] \} ds - \int_{\Omega} \mathbf{p}[s]^T \mathbf{d}[s] ds - \int_{\partial\Omega} \mathbf{f}[s]^T \mathbf{d}[s] ds, \quad (7)$$

where  $\Omega$  is the fiber support domain;  $\mathbf{t}$  are generalized strengths,  $\mathbf{d}$  displacements,  $\mathbf{p}$  interior loads, and  $\mathbf{f}$  boundary loads, all associated with the fiber  $\mathcal{S}[s]$ ;  $\mathbf{H}$  is a compliance operator such that  $\frac{1}{2} \mathbf{t}^T \mathbf{H} \mathbf{t}$  is the local contribution to the complementary energy; and  $s$  is a material abscissa varying in  $\Omega$ . The ICM actually provides appropriate objective definitions for  $\mathbf{t}[s]$ ,  $\mathbf{d}[s]$ , and  $\mathbf{H}[s]$ , as a generalization of quantities used in the corresponding linear modeling, and an explicit expression for the nonlinear displacement-to-strain relationship  $\boldsymbol{\varrho}[\mathbf{d}[s]]$ .

By partitioning the structure in finite elements and assuming in each of them both the internal fields  $\mathbf{t}[s]$  and  $\mathbf{d}[s]$  defined as functions of a discrete set of tensions and displacement element parameters  $\mathbf{t}_e$  and  $\mathbf{d}_e$ ,

$$\mathbf{t}[s] := \mathbf{t}[s, \mathbf{t}_e], \quad \mathbf{d}[s] := \mathbf{d}[s, \mathbf{d}_e], \quad (8)$$

expression (7) can be reduced to an algebraic form suitable for use in a numerical solution procedure.

**3.1. Element interpolation in linear analysis.** In linear analysis we usually assume a linear relationship

$$\mathbf{t}[s] := \mathbf{B}_t[s] \mathbf{t}_e, \quad \mathbf{d}[s] := \mathbf{B}_d[s] \mathbf{d}_e, \quad (9a)$$

with  $\mathbf{B}_t[s]$  and  $\mathbf{B}_d[s]$  collecting the interpolation shape functions. Due to the linear relationship between  $\mathbf{d}[s]$  and  $\boldsymbol{\varrho}[s]$ , we also obtain a linear interpolation for the strain

$$\boldsymbol{\varrho}[s] = \mathbf{B}_\varepsilon[s] \mathbf{d}_e. \quad (9b)$$

As a consequence, performing integration, virtual works equation (1) can be rewritten in FEM format:

$$\sum_e \mathcal{A}_e \left( \begin{bmatrix} -\mathbf{H}_e & \mathbf{D}_e \\ \mathbf{D}_e^T & \cdot \end{bmatrix} \begin{bmatrix} \mathbf{t}_e \\ \mathbf{d}_e \end{bmatrix} - \begin{bmatrix} \cdot \\ \mathbf{p}_e \end{bmatrix} \right) = \mathbf{0}, \quad (10a)$$

where  $\mathcal{A}_e$  is the standard FEM assemblage operator, summation is extended to all elements in the partition, and the element matrices  $\mathbf{H}_e$  and  $\mathbf{D}_e$  and vector  $\mathbf{p}_e$  are defined by

$$\mathbf{H}_e := \int_e \mathbf{B}_t[s]^T \mathbf{H}[s] \mathbf{B}_t[s] ds, \quad \mathbf{D}_e := \int_e \mathbf{B}_t[s]^T \mathbf{B}_\varepsilon ds, \quad \mathbf{p}_e := \int_e \mathbf{B}_d[s]^T \mathbf{p}[s] ds. \quad (10b)$$

Stress and displacement interpolations can be set independently (we only need to satisfy the well-known Brezzi–Babuska condition [Babuška 1971; Brezzi 1974]); in this case we call this a *mixed interpolation*. Frequently they are related to each other by assuming

$$\mathbf{t}[s] = \mathbf{H}[s]^{-1} \mathbf{B}_\varepsilon[s] \mathbf{d}_e. \quad (11)$$

This choice, called *compatible interpolation*, implicitly satisfies the elastic laws  $\mathbf{t}[s] = \mathbf{H}[s]^{-1}\boldsymbol{\rho}[s]$ , so allowing (10a) to be further simplified into

$$\sum_e \mathcal{A}_e (\mathbf{K}_e \mathbf{d}_e - \mathbf{p}_e) = \mathbf{0}, \quad (12a)$$

where

$$\mathbf{K}_e := \int_e \mathbf{B}_\varepsilon[s]^T \mathbf{H}[s]^{-1} \mathbf{B}_\varepsilon[s] ds. \quad (12b)$$

Accuracy provided by this discretization process, in both its mixed and compatible versions, depends on an appropriate choice for the interpolation matrices  $\mathbf{B}_t[s]$  and  $\mathbf{B}_d[s]$  which have to reproduce as well as possible the expected solution, a locking being produced by inappropriate choices. However there is great experience in this field and a large number of interpolation functions are available in the literature, based on known properties of the expected solutions.

**3.2. Element interpolation in nonlinear analysis.** To transfer this experience from linear to nonlinear analysis is not straightforward. Even taking a linear relationship between the internal fields  $\mathbf{t}[s]$  and  $\mathbf{d}[s]$  and the external element parameters, as expressed by (9a), the expression for  $\boldsymbol{\rho}[s]$  will become nonlinear:

$$\boldsymbol{\rho}[s] := \boldsymbol{\rho}[s, \mathbf{d}_e], \quad (13)$$

because of the nonlinearity between  $\mathbf{d}[s]$  and  $\boldsymbol{\rho}[s]$ . This also implies (10a) will become nonlinear, that is,

$$\mathbf{r} := \sum_e \mathcal{A}_e \left( \begin{bmatrix} -\mathbf{H}_e \mathbf{t}_e + \boldsymbol{\rho}_e[\mathbf{d}_e] \\ \mathbf{D}_e[\mathbf{d}_e]^T \mathbf{t}_e - \mathbf{p}_e \end{bmatrix} \right) = \mathbf{0}, \quad (14)$$

$\boldsymbol{\rho}_e[\mathbf{d}_e]$  and  $\mathbf{D}_e[\mathbf{d}_e]$  being defined by

$$\boldsymbol{\rho}_e[\mathbf{d}_e] := \int_e \mathbf{B}_t[s]^T \boldsymbol{\rho}[s, \mathbf{d}_e] ds, \quad \mathbf{D}_e[\mathbf{d}_e] := \int_e \mathbf{B}_t[s]^T \left[ \frac{\partial \boldsymbol{\rho}[s, \mathbf{d}_e]}{\partial \mathbf{d}_e} \right] ds, \quad (15)$$

and its solution requires the numerical strategies described in Section 2. Difficulties arise from the fact that slender elements, such as beams (or shells), generally have different behavior in the axial (or in-plane) direction than in transversal directions, the former being governed by the elongation of the element, the latter by its bending. As a consequence, the expected solution will be characterized by different shapes for the axial (in-plane) and transversal components of the displacements, which involves different requirements for the corresponding interpolation functions.

We can easily satisfy these requirements in linear analysis. For instance, by referring to the simple case of a planar beam element subjected to nodal loads, the standard interpolation, linear for the axial displacement, cubic for the transversal displacements, and quadratic for the rotations, could be appropriate in linear analysis. The same interpolation could hardly be applied in nonlinear analysis because of local changes in the orientation of the beam axis produced by the beam motion. In fact, due to finite element rotations, the two interpolations become coupled and, as a consequence of the high axial-to-transversal stiffness ratio, which is generally of some orders of magnitude, can produce a strong locking in the discretization. Moreover, in nonlinear analysis we have to be careful in using an appropriate representation for the rotations in order to assure full geometrical coherence in both the

internal description of the element and in the interelement continuity conditions. This can prove to be a difficult task when three-dimensional rotations are involved (see [Ritto-Corrêa and Camotim 2002] and references therein). As recalled in [Garcea et al. 2012, §3.1], rotations are characterized by a second-order orthogonal tensor  $\mathbf{R} \in \mathcal{SO}(3)$  and combine with a product rule, so this is not easy to manage. To refer to its axial vector  $\boldsymbol{\varphi} := \text{spin}(\mathbf{R})$ , nonlinearly related to  $\mathbf{R}$  through Rodrigues' formula (see (17)), could be a convenient choice, but this introduces a nonlinearity in the interpolation of translation components of the displacement when they are expressed in terms of rotational parameters and prevents its definition by a simple linear expression.

To avoid these inconveniences the interpolation law should assure frame invariance in the displacement representation and, moreover, interpolations for the translational and rotational components of the displacement should be separately defined. The use of a mixed interpolation could help in this because the components of  $\mathbf{t}$  are aligned to the material and so they are frame-independent by definition. This makes it possible to express  $\mathbf{t}[s]$  as a linear function of the discrete vector  $\mathbf{t}_e$  when using a mixed interpolation. By appropriate choices for  $\mathbf{B}_t[s]$  we can also filter out, in the virtual works expression  $\int \mathbf{t}[s]^T \boldsymbol{\varrho}[s] ds$ , undesirable aspects of the strain interpolation  $\mathbf{B}_\varepsilon[s]$ . All these possible advantages are lost when using compatible interpolations.

Several techniques can be used in the displacement interpolation to avoid locking, for instance: assuming the same shape functions for the three components of the translation (and/or the rotation) vector, as in the plate element used in [Lanzo et al. 1995; Lanzo and Garcea 1996]; assuming separate interpolations for rotations and translations, as in the beam element used in [Salerno and Lanzo 1997], and assuming a stress interpolation which renders matrix  $\mathbf{D}_e$  independent of translation interpolation, as in [Garcea et al. 1998; 1999]; and filtering the rigid rotations of the element through an appropriate setting of the element reference frame.

All these devices will be implemented in the element formulations proposed in Sections 4 and 5.

**3.3. Updated Lagrangian or corotational interpolation.** A general way to obtain a frame-independent interpolation is to refer to an appropriate reference frame able to filter rigid rotations of the element. Two different strategies can be followed to achieve this objective: first, assuming a Lagrangian description but using an appropriate updating scheme to redefine the reference framing according to the current element alignment; second, using a corotational description, that is, assuming a reference frame which follows the element motion maintaining its alignment.

While being essentially different, the two descriptions use the same scheme, based on a standard change in the observer rule:

$$\bar{\mathbf{d}}_e := \mathbf{g}_e[\mathbf{d}_e], \quad (16a)$$

to translate the element displacement vector  $\mathbf{d}_e$ , referring to a global frame defined once and for all in the analysis, to its representation  $\bar{\mathbf{d}}_e$  in the current element frame. They also use the same displacement interpolation in locally aligned components:

$$\bar{\mathbf{d}}[s] := \mathbf{B}_d[s] \bar{\mathbf{d}}_e. \quad (16b)$$

However, in the (updated) Lagrangian description, the element frame is assumed as fixed (while frequently updated), so (16a) states a linear relationship between  $\mathbf{d}_e$  and  $\bar{\mathbf{d}}_e$ , that is,

$$\mathbf{g}_e[\mathbf{d}_e] := \mathbf{Q}_e[\mathbf{d}_e^R] \mathbf{d}_e, \quad (16c)$$

where  $\mathbf{d}_e^R$  defines the reference configuration and matrix  $\mathbf{Q}_e[\cdot]$  expresses the difference in alignment between the global and local frames. Conversely, in the corotational description, the element frame is assumed to move with the element and then the vectorial function  $\mathbf{g}_e[\mathbf{d}_e] := \mathbf{Q}_e[\mathbf{d}_e]\mathbf{d}_e$  states a nonlinear relation between  $\mathbf{d}_e$  and  $\bar{\mathbf{d}}_e$ .

Note that, while in the former case all nonlinearities of the problem are contained in the internal element description through functions  $\mathbf{q}_e[\bar{\mathbf{d}}_e]$  and  $\mathbf{D}_e[\bar{\mathbf{d}}_e]$ , in the latter case the internal description is decoupled from the external nonlinearities due to the finite rigid rotation of the element, which is taken into account by  $\mathbf{g}_e[\mathbf{d}_e]$ . As a consequence, in the corotational approach the need for an accurate modeling of the element could be somewhat relaxed. In fact, internal displacements, ruled by  $\bar{\mathbf{d}}_e$ , are only related to the element distortion and so, by mesh refinement, they can be made small enough to allow the use of the same interpolation laws derived from the linear analysis, without introducing noticeable interpolation locking. The smallness of  $\bar{\mathbf{d}}_e$  also allows an evaluation of the strain/displacement relationships  $\mathbf{q}[\bar{\mathbf{d}}]$  through its Taylor expansion without noticeable loss in accuracy. A second-order, or even first-order, expansion can be sufficient with fine meshes. In this case, the element description will coincide, in the corotational framing, with that already used in the linear or the so-called second-order analysis, so allowing a direct reuse of standard software libraries widely available for these contexts. This is a great advantage, as pointed out in the pioneering paper [Rankin and Nour-Omid 1988], which is the reason for the diffusion of the corotational approach in the literature (see [M. and C. 2002; Chen et al. 2006; Alsafadie et al. 2010; 2011], to only cite recent proposals), but it is paid for by the need for some complex algebra to obtain derivatives of the nonlinear function  $\mathbf{g}_e[\mathbf{d}_e]$  which are involved in the variations of the strain energy. These can be obtained in standard recursive form as shown in [Garcea et al. 2009], but in any case their derivation adds an extra cost to the analysis.

This extra cost and the need for an appropriate mesh refinement is the weak point of corotational approach. The Lagrangian approach does not have these disadvantages but, conversely, requires a full accurate modeling of the element: that is, it needs an appropriate choice for the structural model to be used in the discretization and a careful setting of interpolation laws. Geometrical coherence plays an important role in path-following and, even more, in asymptotic analysis, and we have to be very careful. The need for an appropriate modeling could be a serious drawback, in general, but the possibility of obtaining geometrically exact models through the ICM procedure described in [Garcea et al. 2012] allows us to eliminate the problem and makes particularly convenient the Lagrangian approach. The beam and shell elements proposed in Sections 4 and 5 are both based on a Lagrangian interpolation.

**3.4. Mixed or compatible format.** We know, from previous discussions, that a mixed interpolation can be really convenient in nonlinear analysis. Consider however that the assumption of a mixed or a compatible interpolation does not necessarily imply the use of a mixed or compatible format in the problem description as it might seem by (10) and (12). In fact, the two formats only differ in the writing of the system of equations in terms of the stress and displacement unknowns or the displacement unknowns alone. We can change from a mixed to a compatible format simply by expressing the stress variables in terms of the displacement unknowns or, conversely, change from a compatible format to a mixed one by splitting the system and explicitly introducing the stress unknowns and their relations to the displacement unknowns. The rewriting does not change the nature of the element, only the external format of its description.

Mixed and compatible formats, while completely equivalent in principle, behave very differently when implemented either in path-following or asymptotic solution strategies. This is an important, if frequently misunderstood, point in practical computations which has been widely discussed in [Garcea et al. 1998; 1999]. We refer readers to these papers and to the general discussion given in [Casciaro 2005] for more details, and only recall here that both numerical strategies described in Section 2 need the function  $\mathbf{K}[\mathbf{u}]$  to be appropriately smooth in its controlling variables  $\mathbf{u}$ . In path-following analysis, its smoothness will imply having  $\mathbf{K}[\mathbf{u}] \approx \tilde{\mathbf{K}} := \mathbf{K}[\mathbf{u}_0]$  when  $\mathbf{u}$  moves in the neighborhood of  $\mathbf{u}_0$  of interest, so allowing a fast convergence of the Newton iterative process. Analogously, the matrix  $\mathbf{K}[\mathbf{u}]$  being the Hessian of the strain energy, its smoothness implies, in asymptotic analysis, that the higher-order energy term neglected in the fourth-order expansion (6h) be really irrelevant, so allowing an accurate recovery of the equilibrium path. We know that the smoothness of a nonlinear function strictly depends on the choice of the set of its control variables, that is, on the format of its description, and can change noticeably when referring to another, even corresponding, set. As a consequence, the mixed and compatible formats, even if referring to the same problem, can be characterized by a different smoothness and so behave differently in practice, when used within a numerical solution process. Actually, the compatible format is particularly sensitive to what we call *extrapolation locking* in [Garcea et al. 1998; 1999] which can produce a loss of convergence and then a premature arrest of the incremental process, when used in path-following analysis, or unacceptable errors in the path recovery, when used in asymptotic analysis. These inconveniences are easily avoided by changing to a mixed format.

#### 4. A nonlinear beam element based on Saint-Venant general theory

A finite element for the three-dimensional nonlinear beam model, derived from Saint-Venant general rod theory through ICM (see [Garcea et al. 2012, §5]), will be described here. The model accounts for shear deformability and section warping due to the helicoid distortion due to torsion, that is, the so-called Wagner effect. A separate (mixed) interpolation is used for section strengths  $\mathbf{t}[s]$  and displacements  $\mathbf{d}[s]$ ,  $s$  being a material abscissa along the beam axis. The element has been implemented into a computer code, named COBE (see [Madeo 2008]), aimed at nonlinear analysis of three-dimensional beam assemblages using either asymptotic or the path-following strategies.

**4.1. Some preliminaries on rotation algebra.** Before entering into element definition we need to specify how rotation tensors are managed. In fact, we need to refer to a suitable parametrization which allows the configuration to be described in terms of variables belonging to a linear manifold as required by the formulation presented in Section 2, in order for the strain energy variations to be evaluated accurately through standard directional derivatives (see [Garcea et al. 2009]).

Finite three-dimensional rotations can be directly described in terms of a proper orthogonal tensor  $\mathbf{R}$ , that is a member of the nonlinear manifold  $\text{SO}(3)$ . In matrix notation, the rotation tensor  $\mathbf{R}$  becomes a  $3 \times 3$  orthogonal matrix that, by exploiting the orthogonality property  $\mathbf{R}^{-1} = \mathbf{R}^T$ , is a function of only three parameters. A useful way to express  $\mathbf{R}$  in terms of quantities lying in a linear manifold is that of [Rodrigues 1840]:

$$\mathbf{R}[\varphi] = \mathbf{I} + \frac{\sin \varphi}{\varphi} \mathbf{W}[\varphi] + \frac{(1 - \cos \varphi)}{\varphi^2} \mathbf{W}^2[\varphi], \quad (17)$$

which uses the rotation vector  $\boldsymbol{\varphi} = [\varphi_1, \varphi_2, \varphi_3]^T$ ,  $\varphi = \sqrt{\varphi_1^2 + \varphi_2^2 + \varphi_3^2}$  being its magnitude and  $\mathbf{W}[\boldsymbol{\varphi}] := \text{spin}(\boldsymbol{\varphi})$  the associated spin matrix. This representation uses a minimal set of parameters, is singularity free, and gives a one-to-one correspondence in the range  $0 \leq \varphi < 2\pi$  (see [Ritto-Corrêa and Camotim 2002]). Taking  $\boldsymbol{\varphi} := \boldsymbol{\varphi}[s]$ , it is also useful to introduce the operator

$$\mathbf{T}[\boldsymbol{\varphi}] := \mathbf{I} + \frac{1 - \cos \varphi}{\varphi^2} \mathbf{W}[\boldsymbol{\varphi}] + \frac{\varphi - \sin \varphi}{\varphi^3} \mathbf{W}^2[\boldsymbol{\varphi}], \quad (18a)$$

which satisfies the following equivalence (a comma means partial derivative):

$$\mathbf{R}(\boldsymbol{\varphi})^T \mathbf{R}(\boldsymbol{\varphi})_{,s} = \text{spin}(\mathbf{T}^T[\boldsymbol{\varphi}] \boldsymbol{\varphi}_{,s}). \quad (18b)$$

**4.2. Handling the nonlinear beam model.** By referring to the nonlinear beam model proposed in [Garcea et al. 2012, §5], we consider a beam element, initially straight and of length  $\ell_e$ . The section strengths  $\mathbf{t}$  and work-associated section strains  $\boldsymbol{\varrho}$  are defined as

$$\mathbf{t} := \begin{bmatrix} N \\ \mathbf{M} \end{bmatrix}, \quad \boldsymbol{\varrho} = \boldsymbol{\varrho}_L + \boldsymbol{\varrho}_Q, \quad (19a)$$

$N$  and  $\mathbf{M}$  being the vectors collecting the axial/shear strengths and torsional/bending couples and

$$\boldsymbol{\varrho}_L := \begin{bmatrix} \boldsymbol{\varepsilon}_L \\ \boldsymbol{\chi}_L \end{bmatrix}, \quad \boldsymbol{\varrho}_Q := \begin{bmatrix} \boldsymbol{\varepsilon}_Q[\boldsymbol{\varrho}_L] \\ \boldsymbol{\chi}_Q[\boldsymbol{\varrho}_L] \end{bmatrix}, \quad (19b)$$

where  $\boldsymbol{\varepsilon}_L$  and  $\boldsymbol{\chi}_L$  are given by

$$\boldsymbol{\varepsilon}_L := \mathbf{R}^T(\mathbf{v}_{,s} + \mathbf{e}_1) - \mathbf{e}_1, \quad \boldsymbol{\chi}_L := \mathbf{T}^T \boldsymbol{\varphi}_{,s}, \quad (19c)$$

as functions of translations  $\mathbf{v}[s]$  and rotations  $\boldsymbol{\varphi}[s]$  associated to a material abscissa  $s$  varying from 0 to  $\ell_e$ , and  $\boldsymbol{\varepsilon}_Q$  and  $\boldsymbol{\varrho}_Q$  collect the linear and quadratic terms in the expression of  $\boldsymbol{\varrho}$  defined by [Garcea et al. 2012, Equation (39)]. The modeling is completed by the compliance operator  $\mathbf{H}$  defined in [Garcea et al. 2012, §5.1].

Note that a large part of the components of  $\boldsymbol{\varrho}_Q$  could refer to numerically negligible effects and so it can be omitted in practical computations (see [Garcea et al. 2012, §5.2.3]). Also note that, when using an appropriate reference frame suitable to render  $\boldsymbol{\varphi} \ll 1$  within the element and making  $\mathbf{W} := \text{spin}[\boldsymbol{\varphi}]$ , we can replace the finite element expressions (17) and (18a) by their Taylor expansions,

$$\mathbf{R}[\boldsymbol{\varphi}] = \mathbf{I} + \mathbf{W} + \frac{1}{2} \mathbf{W}^2 + \frac{1}{6} \mathbf{W}^3 + \frac{1}{24} \mathbf{W}^4 + \dots, \quad \mathbf{T}[\boldsymbol{\varphi}] = \mathbf{I} + \frac{1}{2} \mathbf{W} + \frac{1}{6} \mathbf{W}^2 + \frac{1}{24} \mathbf{W}^3 + \dots \quad (20)$$

**4.3. Mixed finite beam element.** The beam element description starts with the choice of the element reference frame  $\mathbf{x}_e = \{x_1, x_2, x_3\}$ , aligned to the element as will be detailed in the sequel. We denote with  $\mathbf{R}[s]$  and  $\boldsymbol{\varphi}[s]$  the rotation matrix and the corresponding rotation vector relating the alignment of the section  $\mathcal{S}[s]$  to the element frame, and with  $\mathbf{R}_e$  the rotation matrix relating  $\mathbf{x}_e$  to the global frame  $\mathbf{x}_G$  which refers to the overall beam assemblage.

Stress is defined by a linear interpolation for  $\mathbf{M}[s] := \{M_1[s], M_2[s], M_3[s]\}$  while  $N[s] = N_e := \{N_1, N_2, N_3\}$  is assumed as constant over the element. Displacement is defined by a quadratic interpolation for the rotation vector  $\boldsymbol{\varphi}[s] = \{\varphi_1[s], \varphi_2[s], \varphi_3[s]\}$ , and by a linked interpolation for the translation vector  $\mathbf{v}[s] = \{v_1[s], v_2[s], v_3[s]\}$ . As a consequence, the element behavior is controlled by nine stress

parameters  $\{N_e, \mathbf{M}_i, \mathbf{M}_j\}$  and by 15 displacement parameters  $\{\mathbf{v}_i, \mathbf{v}_j, \boldsymbol{\varphi}_i, \boldsymbol{\varphi}_j, \boldsymbol{\varphi}_m\}$ , where indexes  $i$  and  $j$  relate to quantities evaluated in the end-sections of the beam ( $s = 0$  and  $s = \ell_e$ ), and

$$\boldsymbol{\varphi}_m := \frac{1}{\ell_e} \int_0^{\ell_e} \boldsymbol{\varphi}[s] ds. \quad (21)$$

**4.4. Setting of the element frame.** It is convenient to set the element frame  $\mathbf{x}_e$  such that  $\boldsymbol{\varphi}[s]$  is small enough to allow expansions (20). Two different strategies can be used:

- (1) assuming  $\mathbf{x}_e$  as a corotational system moving with the element such that  $\boldsymbol{\varphi}_m$  is identical to zero and
- (2) assuming  $\mathbf{x}_e$  as a fixed system but such that  $\boldsymbol{\varphi}_m = \mathbf{0}$  in some near reference configuration.

The former choice allows the rigid rotations of the element to be accounted for implicitly and so is less demanding of the internal accuracy of the element. For this reason it was made, for instance, in [Garcea et al. 2009], even if it requires some extra algebra. The latter choice, corresponding to a Lagrangian description, is more convenient in the present context due to the use of geometrically exact elements, and will be used here. We can also make the reference configuration coincident with the current one, so satisfying the condition  $\boldsymbol{\varphi}_m = \mathbf{0}$  exactly, through a simple reference updating scheme. In fact, starting from an initial estimate  $\mathbf{R}_e^{(j)}$  of the element alignment, providing  $\boldsymbol{\varphi}_m^{(j)} \neq \mathbf{0}$ , we can obtain the updated evaluation  $\mathbf{R}_e^{(j+1)}$  by the scheme

$$\mathbf{R}_e^{(j+1)} := \mathbf{R}^T[\boldsymbol{\varphi}_m^{(j)}] \mathbf{R}_e^{(j)}, \quad (22)$$

which provides  $\mathbf{R}[\boldsymbol{\varphi}_m^{(j)}] = \mathbf{R}_e^{T(j)} \mathbf{R}_e^{(j+1)}$  and so, for  $\mathbf{R}_e^{(j+1)} \mathbf{R}_e^{T(j)} = \mathbf{I}$  (that is, at convergence),  $\boldsymbol{\varphi}_m^{(j)} = \mathbf{0}$ . The previous updating can be directly coupled with the global iteration schemes used in the analysis, such as the arc-length iteration used in the path-following approach (see (5)) or the iterative eigenvalue search used in asymptotic analysis (see (6c)).

**4.5. Stress interpolation.** It is convenient to rearrange the element stress parameters in the *natural* format (see [Argyris et al. 1979])

$$\mathbf{t}_e := \begin{bmatrix} \mathbf{m}_r \\ \mathbf{m}_s \\ \mathbf{m}_e \end{bmatrix}, \quad \mathbf{m}_r := N\boldsymbol{\ell}, \quad \mathbf{m}_s := \mathbf{M}_j + \mathbf{M}_i, \quad \mathbf{m}_e := \mathbf{M}_j - \mathbf{M}_i; \quad (23a)$$

in this way the stress interpolation is defined as a function of the *element stress vector*  $\mathbf{t}_e$ :

$$\mathbf{N}[s] = \mathbf{B}_n[s] \mathbf{t}_e, \quad \mathbf{M}[s] = \mathbf{B}_m[s] \mathbf{t}_e, \quad (23b)$$

where

$$\mathbf{B}_n := \frac{1}{\ell_e} [\mathbf{I} \quad \cdot \quad \cdot], \quad \mathbf{B}_m := \frac{1}{2} [\cdot \quad -\mathbf{I} \quad \zeta \mathbf{I}], \quad (23c)$$

with  $\zeta := 2s/\ell_e - 1$  being an adimensional abscissa varying from  $-1$  to  $1$  along the beam axis, and  $\mathbf{I}$  and “ $\cdot$ ” the  $[3 \times 3]$  identity and zero matrices, respectively.

**4.6. Displacement interpolation.** The same natural format can be assumed for the displacements by rearranging the relevant element displacement parameters in the *element displacement vector*

$$\mathbf{d}_e := \begin{bmatrix} \boldsymbol{\phi}_r \\ \boldsymbol{\phi}_s \\ \boldsymbol{\phi}_e \\ \boldsymbol{\phi}_m \end{bmatrix}, \quad \begin{aligned} \boldsymbol{\phi}_r &:= (\mathbf{v}_j - \mathbf{v}_i)/\ell_e, & \boldsymbol{\phi}_s &:= (\boldsymbol{\varphi}_j - \boldsymbol{\varphi}_i)/2, \\ \boldsymbol{\phi}_e &:= (\boldsymbol{\varphi}_j + \boldsymbol{\varphi}_i)/2 - \boldsymbol{\varphi}_m, & \boldsymbol{\phi}_m &:= \boldsymbol{\varphi}_m. \end{aligned} \quad (24a)$$

The interpolation law for the rotations will be defined by

$$\boldsymbol{\varphi}[\zeta] = \mathbf{B}_\varphi[\zeta] \mathbf{d}_e, \quad \mathbf{B}_\varphi := [\cdot, \zeta \mathbf{I}, (\frac{3}{2}\zeta^2 - \frac{1}{2})\mathbf{I}, \mathbf{I}]. \quad (24b)$$

The interpolation for translations will be assumed as linked to that of the rotations, according to the following rule:

$$\boldsymbol{\gamma} := \mathbf{v}_{,s}[\zeta] - \text{spin}(\boldsymbol{\varphi}[\zeta])\mathbf{e}_1 = \text{const.} \quad (24c)$$

**4.7. Expression for the complementary energy.** The element contribution to the complementary energy will be expressed in the form

$$\Psi_e := \frac{1}{2} \int_e \mathbf{t}[s]^T \mathbf{H} \mathbf{t}[s] ds = \frac{1}{2} \mathbf{t}_e^T \mathbf{H}_e \mathbf{t}_e. \quad (25a)$$

Substituting stress interpolation (23) into (10b), we obtain an explicit expression for the compliance element matrix  $\mathbf{H}_e$ :

$$\mathbf{H}_e := \frac{1}{12\ell_e} \begin{bmatrix} 12\mathbf{H}_{nn} & -6\ell_e\mathbf{H}_{nm} & \cdot \\ -6\ell_e\mathbf{H}_{nm}^T & 3\ell_e^2\mathbf{H}_{mm} & \cdot \\ \cdot & \cdot & \ell_e^2\mathbf{H}_{mm} \end{bmatrix}. \quad (25b)$$

**4.8. Expression for the strain work.** The element contribution to the strain work will be expressed in the form

$$\mathfrak{W}_e := \int_e \mathbf{t}[s]^T (\boldsymbol{\varrho}_L[s] + \boldsymbol{\varrho}_Q[s]) ds = \mathbf{t}_e^T (\boldsymbol{\rho}_{eL} + \boldsymbol{\rho}_{eQ}), \quad (26a)$$

where  $\boldsymbol{\varrho}_L$  and  $\boldsymbol{\varrho}_Q$  are defined in (19) and  $\boldsymbol{\rho}_{eL}$  and  $\boldsymbol{\rho}_{eQ}$  can be split as

$$\boldsymbol{\rho}_{eL} = \{\boldsymbol{\varrho}_{Lr}, \boldsymbol{\varrho}_{Ls}, \boldsymbol{\varrho}_{Le}\}, \quad \boldsymbol{\rho}_{eQ} = \{\boldsymbol{\varrho}_{Qr}, \boldsymbol{\varrho}_{Qs}, \boldsymbol{\varrho}_{Qe}\}. \quad (26b)$$

Exploiting (19c), (20), (23b), and (24b) we obtain

$$\begin{aligned} \boldsymbol{\varrho}_{Lr} &= \frac{1}{2} \int_{-1}^1 \left\{ \boldsymbol{\gamma} - \mathbf{W} \left( \boldsymbol{\gamma} + \frac{1}{2} \mathbf{w} \right) + \frac{1}{2} \mathbf{W}^2 \left( \boldsymbol{\gamma} + \frac{2}{3} \mathbf{w} \right) - \frac{1}{6} \mathbf{W}^3 \left( \boldsymbol{\gamma} + \frac{3}{4} \mathbf{w} \right) + \dots \right\} d\zeta, \\ \boldsymbol{\varrho}_{Ls} &= - \int_{-1}^1 \left\{ \left( \mathbf{I} - \frac{1}{2} \mathbf{W} + \frac{1}{6} \mathbf{W}^2 - \frac{1}{24} \mathbf{W}^3 + \dots \right) (\boldsymbol{\phi}_s + 3\zeta \boldsymbol{\phi}_e) \right\} d\zeta, \\ \boldsymbol{\varrho}_{Le} &= \int_{-1}^1 \left\{ \left( \mathbf{I} - \frac{1}{2} \mathbf{W} + \frac{1}{6} \mathbf{W}^2 - \frac{1}{24} \mathbf{W}^3 + \dots \right) \zeta (\boldsymbol{\phi}_s + 3\zeta \boldsymbol{\phi}_e) \right\} d\zeta, \end{aligned} \quad (26c)$$

where  $\mathbf{W} := \text{spin}(\boldsymbol{\varphi}[s])$  and  $\mathbf{w} := \mathbf{W}\mathbf{e}_1$ , that is,

$$\mathbf{W} := \mathbf{W}_m + \zeta \mathbf{W}_s + \left( \frac{3}{2}\zeta^2 - \frac{1}{2} \right) \mathbf{W}_e, \quad \mathbf{w} := \mathbf{w}_m + \zeta \mathbf{w}_s + \left( \frac{3}{2}\zeta^2 - \frac{1}{2} \right) \mathbf{w}_e, \quad (26d)$$

with  $W_\beta := \text{spin}(\phi_\beta)$ ,  $w_\beta := W_\beta e_1$ , and  $\beta = m, s, e$ . Constant  $\gamma$ , defined by (24c), is obtained by integrating over the element:

$$\gamma = \phi_r - w_m. \tag{26e}$$

In a similar fashion it is possible to obtain  $\varrho_Q$ ; its complex expression is not reported here, it being more simple and effective to derive it directly using algebraic manipulators.

**4.9. Energy variations.** By combining (25) and (26) we obtain an explicit form for the total strain energy of the element:

$$\Phi_e := \mathcal{W}_e - \Psi_e. \tag{27a}$$

Starting from this expression all energy variations needed by the analysis can be derived by standard algebra. These details, which are easily derived using algebraic manipulators, can be skipped here, and we only recall, as an example for the reader, the expression for the second variation, which is used for defining the tangent stiffness matrix of the element in the mixed format in the simple case where  $\varrho_Q$  is neglected.

Assuming that the reference configuration is straight ( $\varphi_r = \varphi_s = \varphi_e = \mathbf{0}$ ), we obtain

$$\Phi_e'' \dot{u}^2 = \begin{bmatrix} \dot{\mathbf{t}}_e \\ \dot{\mathbf{d}}_e \end{bmatrix}^T \begin{bmatrix} \mathbf{H}_e & \mathbf{D}_e \\ \mathbf{D}_e^T & \mathbf{G}_e \end{bmatrix} \begin{bmatrix} \dot{\mathbf{t}}_e \\ \dot{\mathbf{d}}_e \end{bmatrix}, \tag{27b}$$

where  $\mathbf{H}_e$  is given directly by (25b), and matrices  $\mathbf{D}_e$  and  $\mathbf{G}_e$  are defined by

$$\mathbf{D}_e := \begin{bmatrix} \mathbf{I} & \mathbf{0} & \mathbf{0} & \text{spin}(e_1) \\ \mathbf{0} & -\mathbf{I} & \mathbf{0} & \mathbf{0} \\ \mathbf{0} & \mathbf{0} & \mathbf{I} & \mathbf{0} \end{bmatrix}, \quad \mathbf{G}_e := \begin{bmatrix} \mathbf{0} & \mathbf{0} & \mathbf{0} & -\mathbf{G}_r \\ \mathbf{0} & \frac{1}{3}\mathbf{G}_m & -\frac{1}{2}\mathbf{G}_s & \frac{1}{2}\mathbf{G}_s \\ \mathbf{0} & -\frac{1}{2}\mathbf{G}_s & \frac{1}{3}\mathbf{G}_m & -\frac{1}{2}\mathbf{G}_e \\ -\mathbf{G}_r & \frac{1}{2}\mathbf{G}_s & -\frac{1}{2}\mathbf{G}_e & -\mathbf{G}_m \end{bmatrix}, \tag{27c}$$

where

$$\begin{aligned} \mathbf{G}_r &:= \text{spin}(m_r), & \mathbf{G}_s &:= \text{spin}(m_s), & \mathbf{G}_e &:= \text{spin}(m_e), \\ \mathbf{G}_m &:= (\mathbf{I} - e_1 e_1^T)m_{r1} + \frac{1}{2} \text{spin}(\{0, -m_{r3}, m_{r2}\}). \end{aligned} \tag{27d}$$

**4.10. Global handling of the beam assemblage.** The element vectors  $\mathbf{t}_e$  and  $\mathbf{d}_e$  are related to the global vectors  $\mathbf{t}_G$  and  $\mathbf{d}_G$ , collecting all kinematical and static degrees of freedom of the overall assemblage, that is, the displacements  $\mathbf{u}_G$  and rotations  $\varphi_G$  in all its nodes, and the average rotations  $\varphi_{mG}$  and the stresses  $N_e$ ,  $M_i$ , and  $M_j$  in all its beams. A linear relationship

$$\begin{bmatrix} \mathbf{t}_e \\ \mathbf{d}_e \end{bmatrix} = \mathbf{A}_e \mathbf{d}_G$$

is assumed where matrix  $\mathbf{A}_e$  accounts for the different ordering of variables between the two vectors and for the rotations  $\mathbf{R}_e$  of the element frames with respect to the global frame. In this way we can obtain the relevant matrix, vector, and scalar quantities required by the analysis by a standard assemblage as devised in Section 2.1.

**4.11. Further remarks.** The beam element described here has been built from the interpolation laws (23) and (24). This is one of the simplest choices we could make in order to account for the expected solution. It recovers the exact solution for the linear modeling in the case of a straight reference configuration and zero distributed loads, so it can provide satisfactory accuracy even if using a rough mesh refinement. A better element could be obtained by using higher-order interpolation functions or by referring to specialized interpolation rules able to recover more accurately the main aspects of the nonlinear solution. To refer to the linearized solution, for example, as in [Garcea et al. 1999] for planar beams, could mean a noticeable improvement in the element accuracy and allow rougher meshes. An investigation in this direction, which is outside the scope of the present paper, could be of interest.

## 5. A nonlinear plate element based on Kirchhoff theory

A plate element, based on the nonlinear thin-plate model recovered in [Garcea et al. 2012, §6.6], will be described here. The element has been introduced in the already available code KASP (see [Garcea 2001; Garcea et al. 2002]) aimed at the postbuckling analysis of plate assemblages using either the asymptotic or path-following approaches, according to the solution strategies described in Section 2.

The previous version of the code was based on a mixed version of the well-known von Kármán–Marguerre nonlinear plate model, enriched with the appropriate quadratic kinematical terms related to the in-plane rotations, as described in [Lanzo et al. 1995; Lanzo and Garcea 1996]. This modeling only guarantees second-order accuracy in satisfying frame independence requirements. However, even if exact objectivity is an essential prerequisite in nonlinear analysis, in particular when using an asymptotic approach, the error produced by the code little affects a correct evaluation of the critical and postcritical structural behavior in all the numerical tests referred to in the cited papers. In fact, in most cases examined, the postbuckling behavior was dominated by the strong postbuckling stress redistribution, so making the effects of the objectivity errors quantitatively irrelevant.

As also confirmed in successive papers [Garcea 2001; Garcea et al. 2002] this behavior is typical of box structures built with plate panels, especially when local buckling occurs, but stress redistribution reduces noticeably when modeling slender thin-walled beams as plate assemblages, because of the presence of large global rotations with minimal local distortions. So the use of full objective structural models is needed in these cases and should always be used to assure the general robustness of the code.

**5.1. Handling the nonlinear thin-plate model.** Denoting with  $s := \{X_1, X_2\}$  an in-plane material abscissa, stress and strain in the plate models are characterized by the local strengths  $\mathbf{t}[s] := \{N[s], \mathbf{M}[s]\}^T$ , where  $N := \{N_1, N_2, N_{12}\}$  and  $\mathbf{M} := \{M_1, M_2, M_{12}\}$  collect the membranal strengths and bending couples, respectively, while the work-conjugate strain  $\boldsymbol{\varrho}[s] := \{\boldsymbol{\varepsilon}[s], \boldsymbol{\chi}[s]\}$  is defined in compact form by [Garcea et al. 2012, Equation (54)]. Expanding the products, we obtain

$$\boldsymbol{\varepsilon} = \left\{ \begin{array}{l} u_{,1} + \frac{1}{2}(u_{,1}^2 + v_{,1}^2 + w_{,1}^2) \\ v_{,2} + \frac{1}{2}(u_{,2}^2 + v_{,2}^2 + w_{,2}^2) \\ u_{,2} + v_{,1} + (u_{,1} u_{,2} + v_{,1} v_{,2} + w_{,1} w_{,2}), \end{array} \right\}, \quad (28a)$$

$$\boldsymbol{\chi} = \left\{ \begin{array}{l} w_{,11} + (w_{,11} u_{,1} - u_{,11} w_{,1} - v_{,11} w_{,2} + w_{,11} v_{,2}) + (u_{,2} v_{,11} w_{,1} \\ \quad + u_{,1} w_{,11} v_{,2} - v_{,2} u_{,11} w_{,1} - u_{,1} v_{,11} w_{,2} - u_{,2} w_{,11} v_{,1} + v_{,1} u_{,11} w_{,2}) \\ w_{,22} + (w_{,22} u_{,1} - u_{,22} w_{,1} - v_{,22} w_{,2} + w_{,22} v_{,2}) + (u_{,2} v_{,22} w_{,1} \\ \quad + u_{,1} w_{,22} v_{,2} - v_{,2} u_{,22} w_{,1} - u_{,1} v_{,22} w_{,2} - u_{,2} w_{,22} v_{,1} + v_{,1} u_{,22} w_{,2}) \\ w_{,12} + (w_{,12} u_{,1} - u_{,12} w_{,1} - v_{,12} w_{,2} + w_{,12} v_{,2}) + (u_{,2} v_{,12} w_{,1} \\ \quad + u_{,1} w_{,12} v_{,2} - v_{,2} u_{,12} w_{,1} - u_{,1} v_{,12} w_{,2} - u_{,2} w_{,12} v_{,1} + v_{,1} u_{,12} w_{,2}) \end{array} \right\}, \quad (28b)$$

$u[s]$ ,  $v[s]$ , and  $w[s]$  being the components of the average displacement (translation)  $\mathbf{d}[s]$  of the transversal fiber, according to a fixed frame  $\mathbf{x}_e := \{x_1, x_2, x_3\}$  aligned to the element. Expressions (28) are frame invariant, so the actual choice for this frame is irrelevant for their accuracy, even if it is convenient to refer to the local average alignment of the plate and make  $x_3$  orthogonal to its average plane, for practical reasons. It is worth noting that the Kirchhoff assumption of zero shear deformation allows the rotation parameters to be taken away from the kinematical description, so the nonlinear model is expressed in terms of the displacement fields alone, avoiding the use of a rotation algebra. Also note that the membranal strain  $\boldsymbol{\varepsilon}$  coincides with that of the Green–Lagrange strain tensor, while the curvature  $\boldsymbol{\chi}$  takes a complex expression with respect to the linear approximation assumed in the classical von Kármán–Marguerre theory. The difference lies in the addition of some quadratic and cubic extra terms which take into account pointwise differences in the orientations between the local normal to the middle surface and the  $x_3$  axis. The modeling is completed by the compliance operator

$$\mathbf{H} := \begin{bmatrix} \mathbf{C}_n & \cdot \\ \cdot & \mathbf{C}_m \end{bmatrix}, \quad (28c)$$

$\mathbf{C}_n$  and  $\mathbf{C}_m$  being defined by [Garcea et al. 2012, Equation (51b)].

It is worth mentioning that both the two approximate models, previously implemented in KASP, were based on the same modeling while a linear approximation was used for the curvatures. Membranal strains were defined by the complete quadratic expression (28a) in what we called the *complete Lagrangian* (LC) model and by a simplified expression, which only maintains quadratic terms in  $w$ , in the *simplified Lagrangian* (LS) model. The LS version is characterized by better flexural behavior, so it was the standard option in KASP.

**5.2. Mixed-plate finite element.** The discrete model is based on the high-continuity (HC) finite element interpolation proposed in [Aristodemo 1985], which has also been used in the initial version of KASP. The element was one of the first proposals in the spline interpolation approach (see [Hughes et al. 2005]), and it is very convenient in nonlinear plate analysis. We do not include details of this interpolation, which the reader can find in [Garcea 2001; Garcea et al. 2002] and only recall here that its main advantage is that of assuring interelement continuity for both displacement components and their derivatives, with a minimal use of displacement parameters (approximately three kinematical degrees of freedom per element) and without needing rotational degrees of freedom.

As already done in KASP, a  $[2 \times 2]$  Gauss scheme has been used to integrate all the energy terms required by the analysis. Letting  $s^g$  be the position of the Gauss point  $g$  within the element  $e$  and denoting, from now on, with the index  $g$  quantities evaluated at point  $g$ , the strain energy can be evaluated by Gauss integrations as

$$\Phi_e := \sum_g (\mathcal{W}_g - \Psi_g), \quad (29a)$$

where

$$\Psi_g := \mathbf{t}_g^T \boldsymbol{\rho}_g A_g, \quad \Psi_g := \frac{1}{2} \mathbf{t}_g^T \mathbf{H}_g \mathbf{t}_g A_g, \quad (29b)$$

$\mathbf{H}_g$  being defined by (28c),  $A_g := \frac{1}{4} \ell_1 \ell_2$  the area pertaining to point  $g$ , the Gauss strain  $\boldsymbol{\rho}_g[\mathbf{d}_e] := \{\boldsymbol{\varepsilon}_g, \boldsymbol{\chi}_g\}$  obtained by (28a) and (28b) making  $\mathbf{s} = \mathbf{s}_g$ , and the Gauss point stress  $\mathbf{t}_g := \{N_g, \mathbf{M}_g\}$  defined by

$$N_g = \begin{bmatrix} N_{g11} \\ N_{g22} \\ N_{g12} \end{bmatrix}, \quad \mathbf{M}_g = \begin{bmatrix} M_{g11} \\ M_{g22} \\ M_{g12} \end{bmatrix}, \quad (29c)$$

where  $N_{g11}, N_{g22}, \dots, M_{g12}$  are directly assumed as element parameters controlling the stress interpolation within a mixed format.

This simple integration scheme is generally sufficient for our purpose. Note that, even if more sophisticated interpolations could also be used, this choice provides an exact correspondence with the results obtained in [Lanzo and Garcea 1996; Garcea 2001; Garcea et al. 2002] by allowing attention to be focused on the difference due to the use of a more accurate structural plate model without introducing any disturbing discretization improvement.

The energy variations needed by the analysis can be derived from (29) by standard algebra and assemblage procedures. Explicit expressions, similar to those already given in [Garcea 2001], are simply obtained through the use of algebraic manipulators, so details are not included here.

## 6. Numerical validation

The numerical results are mainly related to the asymptotic analysis, this context being more sensitive to the correctness of both the structural model and its finite element implementation. The results of path-following analysis are based on the same modeling and discretization, while using the corotational updating strategies described in [Garcea 2001; Garcea et al. 2009], so they can be considered very accurate and are used, essentially as a reference to check the accuracy and robustness of the asymptotic results. In all the numerical tests comparisons are performed with results obtained by other authors and/or with analytical solutions, when available.

The proposed three-dimensional beam finite element, implemented into a FEM code named COBE [Madeo 2008], has been tested for compact and general thin-walled cross sections. In all cases the evaluation of the compliance operator  $\mathbf{H}_e$  has been obtained through the solution of the Saint-Venant equations using the FEM approach described in [Petrolo and Casciaro 2004] to which the reader is referred for further details (see also [Lacarbonara and Paolone 2007]). The proposed Kirchhoff plate element has been implemented in the KASP code [Garcea 2001]. In this way, it was easy to compare the results provided by the proposed plate model (denoted as ICM) with those obtained, for the same finite element discretization, using the complete Lagrangian (LC) and simplified Lagrangian (LS) approximate plate models already implemented in the code. Thin-walled beams can be modeled as Saint-Venant rods but also as assemblages of thin plates. This allowed further comparisons between the results provided by the two different models and so made it possible to obtain an independent check on their robustness. The comparison also allows us to emphasize the effects of the Saint-Venant simplifying hypotheses on the boundary conditions and cross-section distortions, in some relevant cases.

The section is organized as follows: First we present some simple tests, with known analytical solutions, showing the improvement in accuracy provided by ICM modeling with respect to the LC and LS models. We then present some tests to show the role played by postbuckling stress redistribution in reducing the accuracy demand in the plate modeling. Next, we present some tests to compare the results obtained for thin-walled structures modeled as beams or as three-dimensional plate assemblages, to show the general accuracy of the beam model recovered by the ICM, as well as its possible shortcomings in the presence of relevant boundary disturbances, local buckling, and in-plane section distortions. Finally, we report some tests referring to multimodal coupled buckling phenomena to show the real effectiveness of the proposed approach in general contexts and complex structural problems.

In the monomodal buckling tests, to compare the accuracy with known solutions, the following quantities, defining the postcritical tangent and curvature to the bifurcated path, have been introduced:

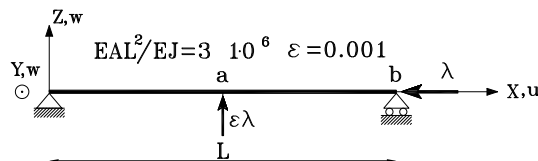
$$\dot{\lambda}_b = -\frac{1}{2} \frac{A_{111}}{A_{011}}, \quad \ddot{\lambda}_b = -\frac{B_{1111} + 3\dot{\lambda}_b B_{0111} + 3\dot{\lambda}_b^2 B_{0011}}{3A_{011}}.$$

**6.1. Accuracy of ICM models.** This numerical investigation focuses on the accuracy of the proposed plate model in contexts where analytical results are available, that is, the simply supported Euler beam and the Roorda frame shown in Figures 1 and 2, respectively.

Despite their simplicity, when analyzed with an asymptotic approach, both problems are taxing with regard to the accuracy of the structural model and its FEM discretization. In fact, in both cases the buckling is not followed by a significant stress redistribution, and in order to obtain the correct postbuckling results the modeling has to assure full objectivity and be free, in its FEM implementation, from both interpolation and extrapolation locking phenomena [Garcea et al. 1999; Salerno and Lanzo 1997]. The two tests have been analyzed using either the beam or the plate modeling and, in the case of the plate modeling, referring to either an in-plane or an out-of-plane buckling. The results are compared with known analytical solutions and with the ones obtained using the approximate LC and LS plate models also implemented in KASP. An independent analysis has also been made using the commercial code ABAQUS [Hibbitt et al. 2007] to investigate the convergence behavior of the proposed elements. In all cases the ICM-beam path-following results are assumed as reference values.

**6.1.1. Euler beam.** The test refers to the Euler beam shown in Figure 1. The resulting paths are drawn in Figure 3 and show a good agreement with those provided by path-following analysis. The values for the buckling load  $\lambda_b$  and the postcritical curvature  $\ddot{\lambda}_b$ , obtained by identifying the expansion parameter  $\xi$  as the end-section rotation of the beam, are reported in Tables 1 and 2, for different discretization meshes.

Note that both the ICM models recover the analytical solution [Salerno and Lanzo 1997]  $\lambda_b = \pi^2$  and  $\ddot{\lambda}/\lambda_b = 0.25$  for sufficiently fine grids exactly. The LC and LS models provide correct answers for the buckling load, but have different postbuckling behavior in the in-plane and out-of-plane analysis: the LC



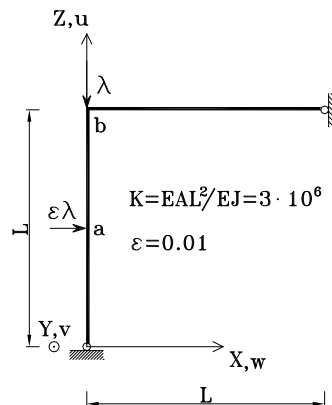
**Figure 1.** Euler beam.

Plate analysis elements		Out-plane buckling			In-plane buckling		
		ICM	S4-R	S8-R	ICM	S4-R	S8-R
$\lambda_b$	16	9.901	9.933	9.868	9.918	33.380	9.868
	32	9.877	9.885	9.868	9.870	14.964	9.867
	64	9.872	9.873	9.868	9.870	10.326	9.867
$\ddot{\lambda}_b/\lambda_b$	16	0.290	.	.	0.332	.	.
	32	0.250	.	.	0.252	.	.
	64	0.250	.	.	0.250	.	.

**Table 1.** Euler beam: plate element convergence.

agrees perfectly with the exact solution in the in-plane case, whereas the LS provides the wrong result  $\dot{\lambda}/\lambda_b = 2$ , eight times greater; conversely, the LS behaves better in the out-of-plane case, by providing the approximation  $\ddot{\lambda}_b/\lambda_b = 0$ , while the LC gives a completely erroneous unstable postbuckling curvature  $\ddot{\lambda}/\lambda_b = -0.75$ . So the LS model could be viewed as a better compromise than the LC, considering the importance of flexural buckling in the slender plates (see also [Lanzo et al. 1995]). Note also, from the results reported in Table 1, the good convergence behavior, in recovering the buckling load, of both the proposed beam and plate elements in comparison with the ones used in ABAQUS (three-node beam element, S4-R, and S8-R plate elements). The improvement in convergence is apparent considering the larger number of variables implied by the ABAQUS meshes: generally more than double in the case of the beam elements while about two to six times greater in the cases of the S4-R and S8-R plate elements.

**6.1.2. Roorda frame.** The test refers to the simple frame shown in Figure 2, first investigated by Roorda. An analytical solution for this problem can be found in [Bazant and L. 1991], by obtaining  $\lambda_b = 13.89$ ,  $\dot{\lambda}_b/\lambda_b = 0.3805$ , and  $\ddot{\lambda}_b/\lambda_b = 0.7576$  by reference to the choice  $\xi := \varphi_b$  for the expansion parameter. These values are recovered exactly by both the ICM models for sufficiently fine meshes (the plate models are analyzed in out-of-plane conditions). The buckling load  $\lambda_b$  and the postbuckling slope  $\dot{\lambda}_b$  are also recovered by the approximate models LC and LS, which, however, provide unsatisfactory results for the



**Figure 2.** Roorda frame.

Beam analysis			
elements	ICM	ICM	ABAQUS
	$\lambda_b$	$\ddot{\lambda}_b/\lambda_b$	$\lambda_b$
4	9.880	0.200	9.880
8	9.870	0.238	9.879
16	9.870	0.246	9.870
32	9.870	0.250	9.870

**Table 2.** Euler beam convergence.

postbuckling curvature  $\ddot{\lambda}_b$ ; we have  $\ddot{\lambda}_b/\lambda_b = 0.2844$  for the LS and an even worse estimate  $\ddot{\lambda}_b/\lambda_b = -1.4352$  for the LC. Note, from Figure 4, that the paths recovered by asymptotic analysis show good agreement with the reference path-following solution, when using both ICM models (they practically coincide up to a transversal displacement  $v_a$  of 10% of the beam length), while the ones obtained by the LC and LS models rapidly deviate with increasing displacement.

A convergence test is also reported in Table 3, including a comparison with the ABAQUS results. Note the good convergence behavior of the ICM model, which confirms that obtained for the Euler beam.

**6.2. The effect of postbuckling stress redistribution.** The poor results of both the LC and LS approximate plate models in the previous examples are a direct consequence of their loss of frame invariance. This however does not imply that these models are wholly inadequate in the nonlinear analysis of slender plates. Actually, they provide a satisfactory recovery of the buckling load  $\lambda_b$  and postbuckling slope  $\dot{\lambda}_b/\lambda_b$  (at least for initially flat plates) and are inaccurate only in the evaluation of the postbuckling curvature  $\ddot{\lambda}_b/\lambda_b$ , which only influences the path recovery at large values of the displacements. Moreover, the previous tests were chosen to represent cases with no or very small postbuckling stress redistribution, which can be considered quite unusual for slender plates. If present, the effect of stress redistributions

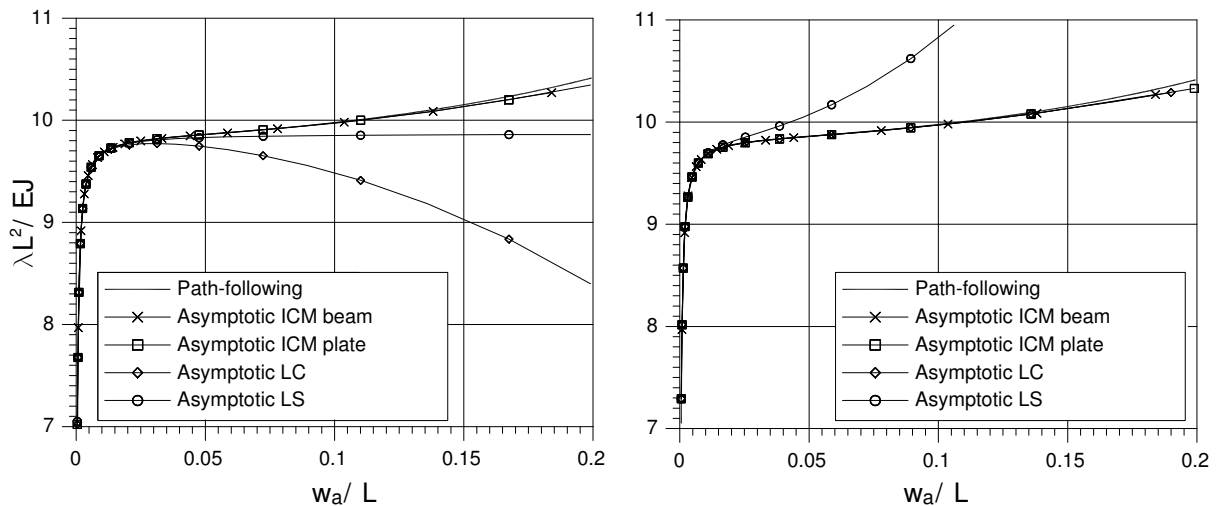


**Figure 3.** Euler beam: out-plane and in-plane equilibrium paths.

	elements	ICM	S4-R	S8-R	Beam
$\lambda_b$	16	13.954	14.005	13.886	
	32	13.903	13.915	13.885	13.886
	64	13.890	13.893	13.884	
$\frac{\dot{\lambda}_b}{\lambda_b}$	16	0.3815	.	.	
	32	0.3807	.	.	0.3805
	64	0.3805	.	.	
$\frac{\ddot{\lambda}_b}{\lambda_b}$	16	0.9070	.	.	
	32	0.7594	.	.	0.7574
	64	0.7570	.	.	

**Table 3.** Roorda frame: convergence test.

dominates the postbuckling behavior, so reducing the relative size of the error.

Stress redistribution can be considered as a typical phenomenon in the postbuckling behavior of slender plates, especially in the case of relevant local buckling effects. We can show several examples for this, but also counterexamples, as in the following tests.

**6.2.1. Simply supported plate subjected to in-plane shear.** The simply supported plate subjected to in-plane shear shown in Figure 5 represents a suitable test case to show the effects of stress redistribution. In fact, in this case, the buckling mode (see Figure 6) implies a large variation of the Gaussian curvature of the middle surface and consequently a strong in-plane distortion of the plate, with relevant postbuckling stress redistribution.

The plate has been analyzed for  $b = 10$ , two different aspect ratios,  $a = 10$  and  $a = 15$ , a boundary shear of  $\tau = \lambda$ , and an imperfection defined by a transversal force  $f = 0.01\lambda$  applied at the center of the plate. The results for both the ICM plate models and the approximate LC and LS models are reported

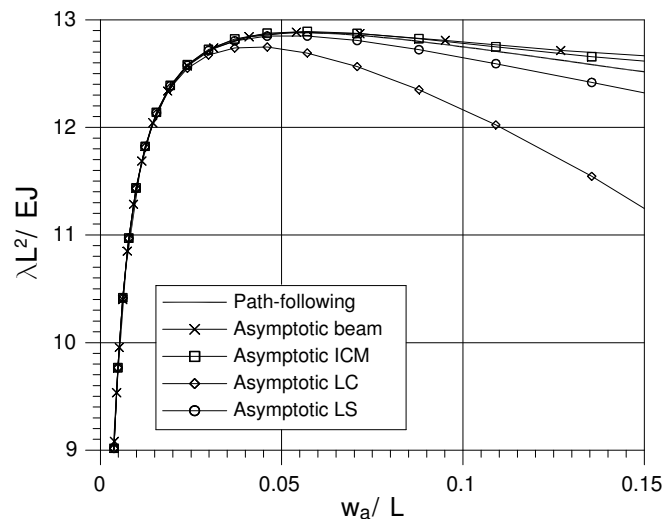


**Figure 4.** Roorda frame: equilibrium path.

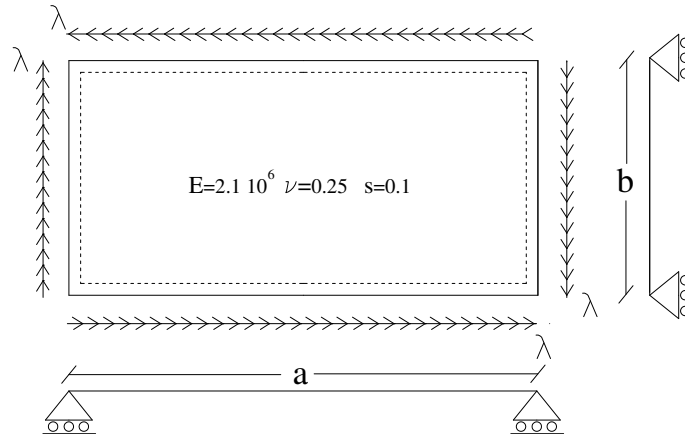


Figure 5. Shear plate: geometry and loads.

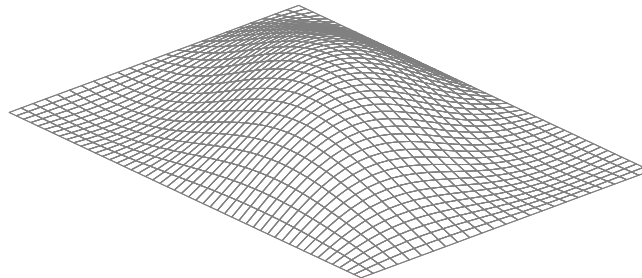


Figure 6. Shear plate: buckling mode ( $a/b = 1.5$ ).

in Figure 7 and Table 4. We obtain from the three models the same evaluations for the buckling load ( $\lambda_b = 171.8$  and  $\lambda_b = 130.3$ ) and the postbuckling curvature ( $\ddot{\lambda}_b = 5.1474$  and  $\ddot{\lambda}_b = 1.053$ , referring to the choice  $\xi := \varphi_b$ ) in the two cases of  $a/b = 1$  and  $a/b = 3/2$ . The ICM versus ABAQUS convergence test reported in Table 4 confirms the good convergence behavior of HC-ICM elements.

Note, from Figure 7, the excellent agreement between the asymptotic and path-following paths for moderate transversal displacements (of the order of the plate depth). As the displacement increases, the asymptotic solution tends to deviate by overestimating the load. This deviation is an expected consequence of the asymptotic approach, because of the omission of higher-order terms in the expansion. The error, which is higher than in the previous test cases, can be related to the importance, in this case, of the stress redistribution process which is largely influenced by corrective modes  $w_{ij}$ , taken into account in (6h) only to within a third-order accuracy (see also the discussion in [Lanzo et al. 1995]).

**6.2.2. C-section cantilever beam.** This second test refers to the cantilever beam with a C-shaped cross section shown in Figure 8, fully clamped at the first edge (by assuming zero displacements and rotations in each point of the section) and subjected to a shear force at the other edge acting at the top of the web. This structure has a flexural/torsional buckling with a minimal section distortion (see Figure 9), which does not involve noticeable postbuckling stress redistributions. As a consequence, the postbuckling curvature will be very sensitive to the accuracy of the nonlinear modeling, as clearly shown in Figure 8,

Convergence for $\lambda_b$ at the mesh refining				
$a/b$	elements	ICM	S4-R	S8-R
1	$9 \times 9$	173.2	186.7	170.6
	$27 \times 27$	172.2	172.5	170.2
	$81 \times 81$	171.8	170.6	170.2
1.5	$9 \times 18$	132.08	139.0	129.53
	$27 \times 54$	130.52	130.69	129.46
	$81 \times 162$	130.28	129.63	129.46

**Table 4.** Shear plate:  $\lambda_b$  convergence.

which shows the paths recovered by asymptotic analysis, using the three considered plate models, in comparison with the reference path-following one. The latter was obtained using an ICM plate that gives results practically coincident with those of ABAQUS. The good agreement between the ICM results and the reference ones is apparent, while both the LC and LS give highly incorrect answers.

**6.2.3. Need for a robust code implementation.** The previous examples show that asymptotic analysis can be very sensitive to even small approximations in frame invariance requirements. Approximate models can give acceptable results in appropriate contexts, but we need to examine the suitability of the context in advance, or, at least, verify the reliability of the results provided by the analysis. Obviously this is unacceptable in a code aimed at general use and, in order to obtain a robust code implementation, we need to use models which are definitely free from objectivity errors such as those we can set up with the ICM procedure.

**6.3. Saint-Venant beam versus Kirchhoff plate modeling.** Tests presented in this subsection compare results from the beam and plate ICM models for thin-walled structures. They show the general accuracy

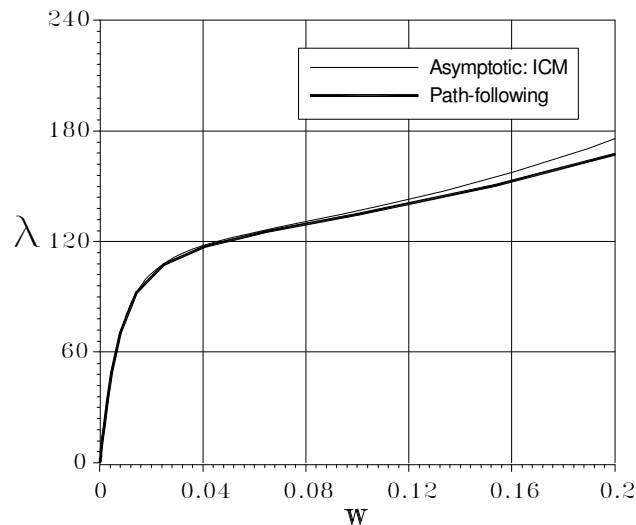


**Figure 7.** Shear plate: equilibrium paths.

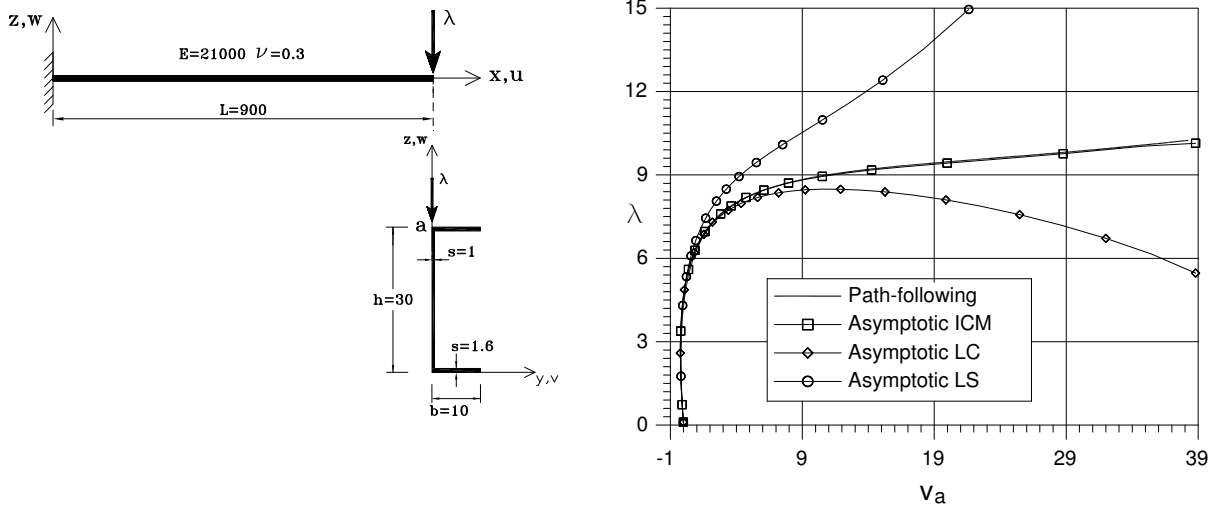


**Figure 8.** Cantilever beam subjected to shear force: geometry and equilibrium path.

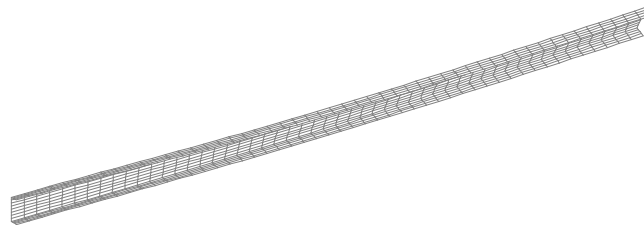


**Figure 9.** Cantilever beam in Figure 8: buckling mode.

of the proposed beam model with respect to the plate reference solution, but also some differences arising from the presence of relevant boundary disturbances or in-plane distortion of the section which cannot be modeled by Saint-Venant one-dimensional theory.

**6.3.1. Clamped C-section beam under compression or shear.** The first test regards the cantilever beam with a C-shaped cross section, shown in Figure 10. The beam has been analyzed for two loading conditions: the first refers to a compressive force and to a small transversal imperfection, both applied at the barycenter of the free edge section; the second refers to a shear force applied at the same point. In the plate analysis, the loading conditions are described by a constant compressive stress in the overall end section and by a constant shear stress in the web, respectively. In both cases an appropriate constant shear is added in the flanges to reproduce the assigned resultants. The boundary constraints are described either by assuming zero displacements and rotations in all points of the clamped section (full clamped), or by assuming zero displacements and rotations in the web and a stress distribution in the flanges corresponding to the one obtained by the Saint-Venant solution (SV clamped). The latter assumption can be considered more adequate for reproducing the Saint-Venant clamping condition in the shear test. Relatively fine element meshes are utilized for both the beam and plate analyses (16 beam elements and  $(5 + 10 + 5) \times 50$  plate elements, respectively) to avoid interference from discretization errors. In all

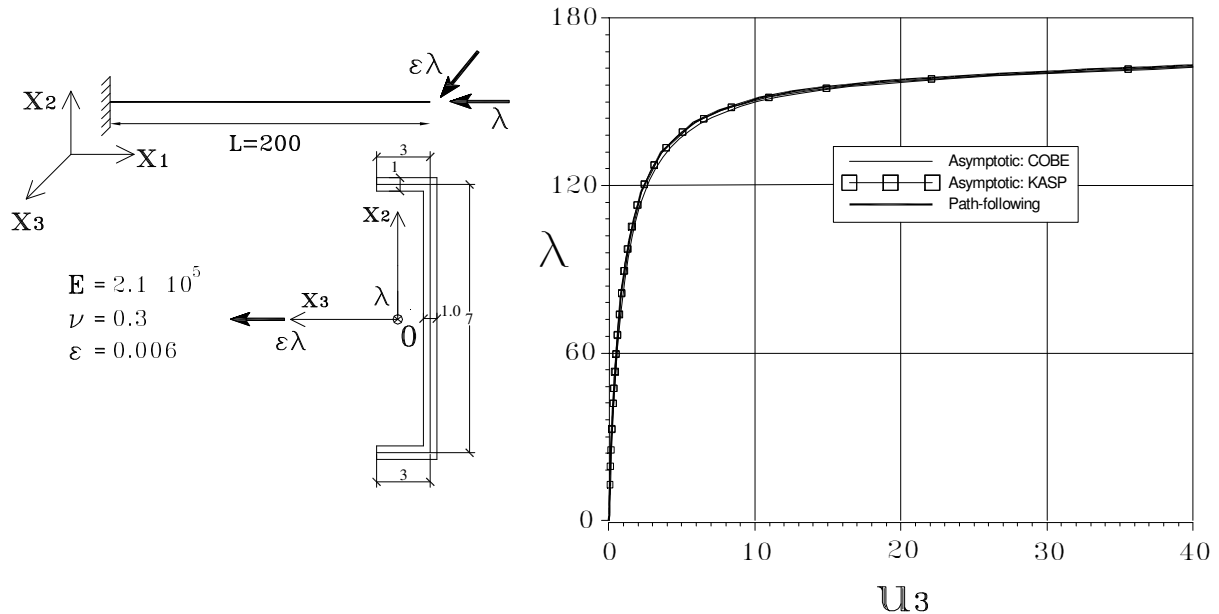


**Figure 10.** C-beam under axial force: geometry and equilibrium paths.

cases, the path-following results were practically coincident with those provided by asymptotic analysis, at least in the range considered, so their plots were generally omitted.

In the compression test, flexural buckling occurs (see Figure 11) at  $\lambda_b = 164.17$ , coincident with the analytical solution in [Bazant and L. 1991], for both the beam and plate analyses. We also obtain an excellent agreement between the beam and the two plate solutions, which are practically coincident, in the recovery of the equilibrium path, as shown in Figure 10, by reference to the transversal components of the edge displacement (in the plate case, the plot refers to the average displacement of the edge section).

When considering the results of the shear test, some differences can be seen in Figures 12 and 13, between the results from the ICM plate and beam models, even if the elastic compliance matrix of the beam section is evaluated by the procedure described in [Petrolo and Casciaro 2004] and so the beam

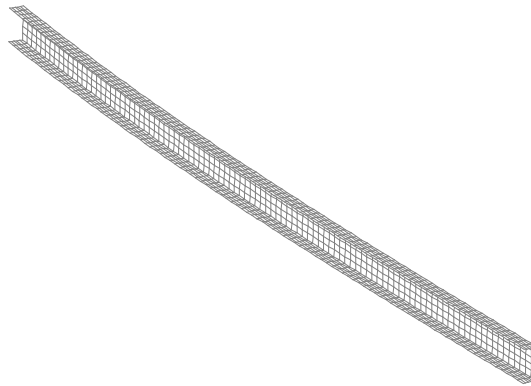


**Figure 11.** C-beam under axial force: buckling mode.

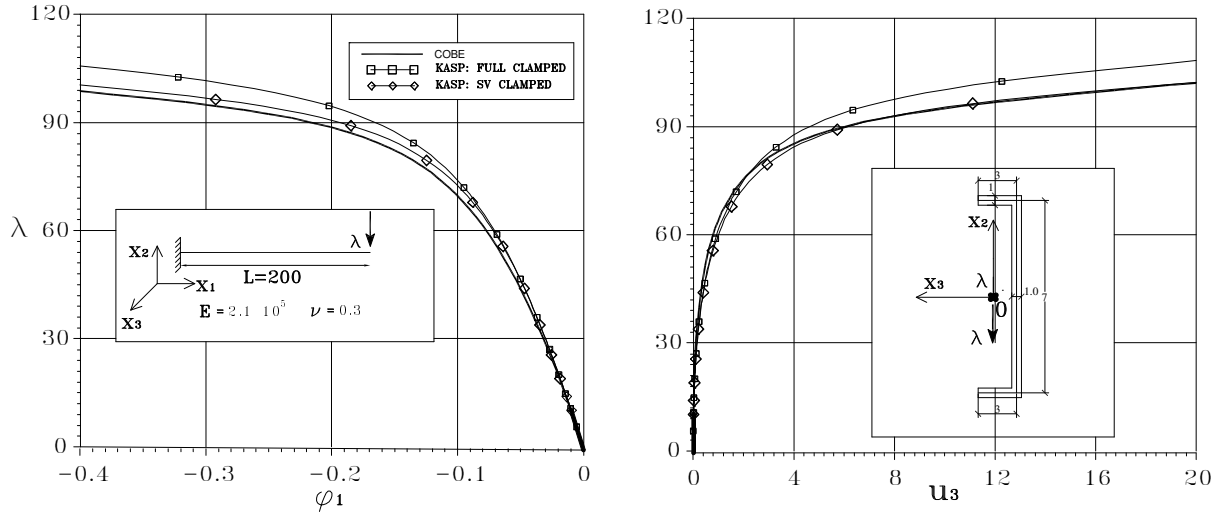


Figure 12. C-beam under shear force: geometry and equilibrium paths.

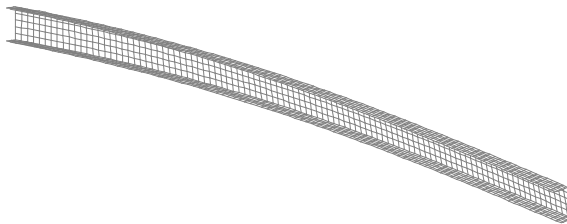


Figure 13. C-beam under shear force: buckling mode.

modeling correctly accounts for all Saint-Venant couplings between shear and torsion. Moreover, in the case of plate analysis, the results are very sensitive to the boundary constraint details. Note that we have a quite large difference, 6%, between the beam and plate results in both the  $\lambda/u_3$  and  $\lambda/\varphi$  curves, when considering full clamped constraints. This difference reduces noticeably when considering SV clamped constraints, even if a residual error still remains in the  $\lambda/\varphi$  plot, which could refer to the overestimate of the torsional flexibility in the Saint-Venant beam solution caused by the omission of the increment in torsional stiffness due to Vlasov’s nonuniform torsion.

**6.3.2. Z-shaped section beam under axial/shear forces.** To appropriately relate boundary constraints for the beam and plate models is even more difficult in the case of nonsymmetric sections, as shown by the two test-cases shown in Figures 14 and 16. Both refer to the same cantilever beam with Z-shaped section, with a compressive or a shear force applied at the centroid of the edge section. As before, relatively fine element meshes have been used in both the beam and plate analyses ( $16$  beam elements and  $(5 + 10 + 5) \times 100$  plate elements) to avoid the influence of discretization errors, and, in the case of the plate, both full clamped and SV clamped have been considered.

In the compressive test, flexural buckling (see Figure 15) occurs at  $\lambda_b = 24.371$  for both beam and plate modeling. Plate analysis is practically uninfluenced by the two different boundary conditions. An excellent agreement can also be seen in the equilibrium paths shown in Figure 14.

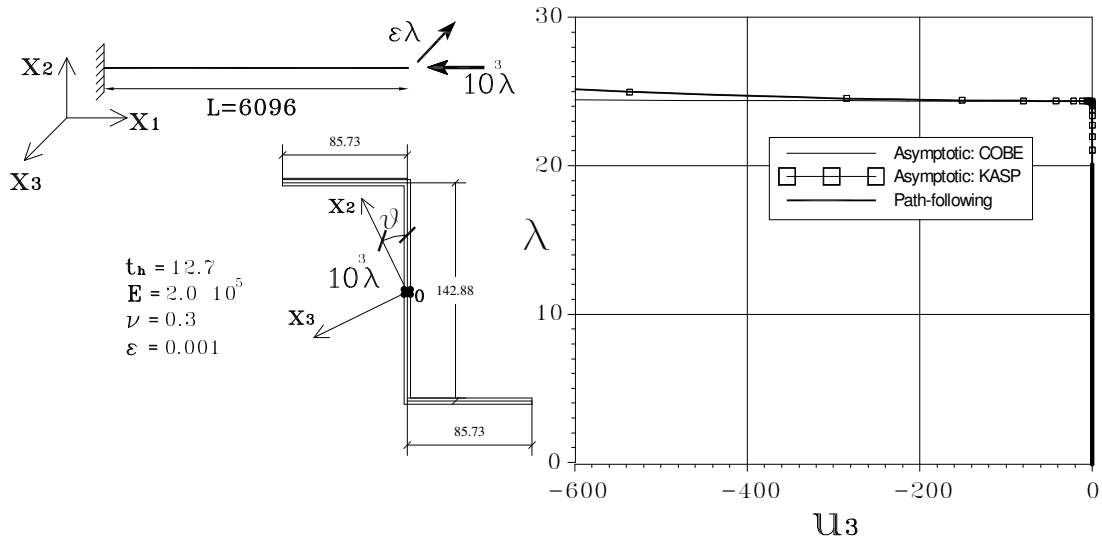


Figure 14. Z-beam under axial force: geometry and equilibrium paths.

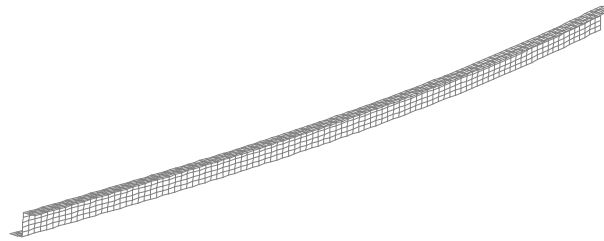


Figure 15. Z-beam under axial force: buckling mode.

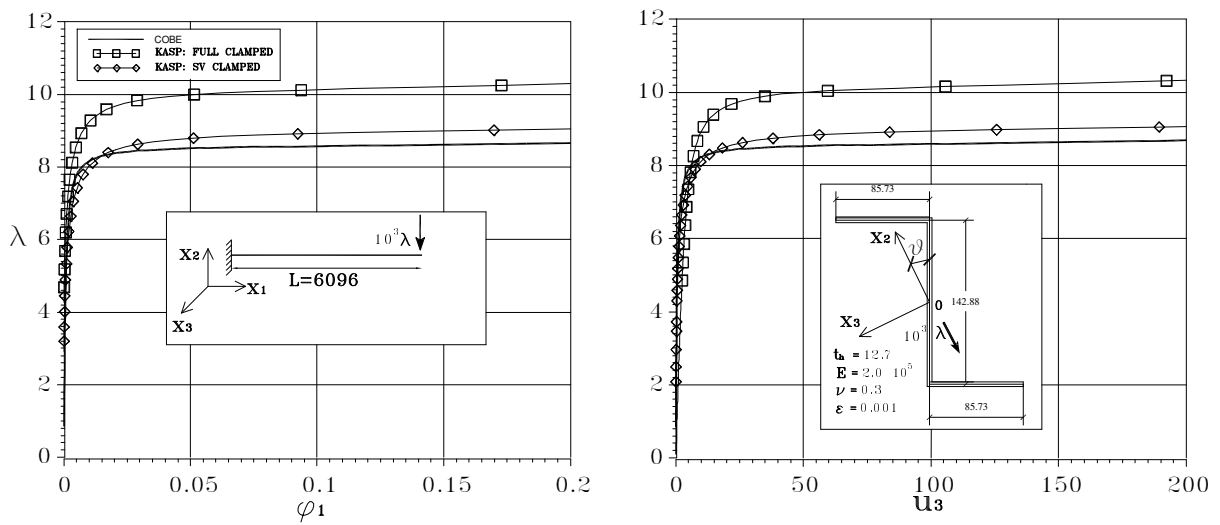


Figure 16. Z-beam under shear force: geometry and equilibrium paths.

Conversely, in the shear test (see Figure 17), we can see from the path comparisons shown in Figure 16 a large difference between the plate and beam models. This is apparent in the full clamped case, which has an error of about 18%, but is also present in the SV clamped case, with an error of 4%, perhaps related to a residual difference in boundary constraints between the plate and beam models or/and to the omission of the Vlasov increment of torsional stiffness in the Saint-Venant beam modeling.

**6.3.3. Wagner effect: flexural/torsional buckling in a compressed T-section cantilever.** The quadratic component  $\chi_Q$  of the section strain defined in [Garcea et al. 2012] accounts for the Wagner axial-torsional nonlinear coupling. This effect could be important in compressed thin-walled beams exploiting flexural/torsional buckling. As an example of this, we refer to the cantilever beam with a T-shaped cross section shown in Figure 18. The analysis has been performed for two different beam lengths,  $L_1 = 300$  and  $L_3 = 500$ , using both the ICM beam and plate FEM models. The latter, based on a refined  $(4 + 8 + 4) \times 41$  plate element mesh and on the assumption of full clamped constraints, can be assumed as reference. The beam model uses eight beam elements and the analysis is repeated with (Q-ICM) or without (L-ICM) the quadratic term  $\chi_Q$ , as an expression of the ICM strain (19). In all cases a flexural/torsional buckling is recovered, as shown in Figure 19.

A notable difference in path recovery is obtained from the three FEM models, as shown in Figure 18 and Table 5. Neither of the two beam solutions recovers the reference plate result exactly. The largest discrepancy occurs for the L-ICM solution as a consequence of the loss of the Wagner coupling. A residual error is however present also in the Q-ICM solution, which could be related to in-plane distortion

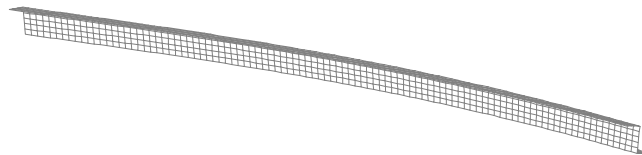


Figure 17. Z-beam under shear force: buckling mode.

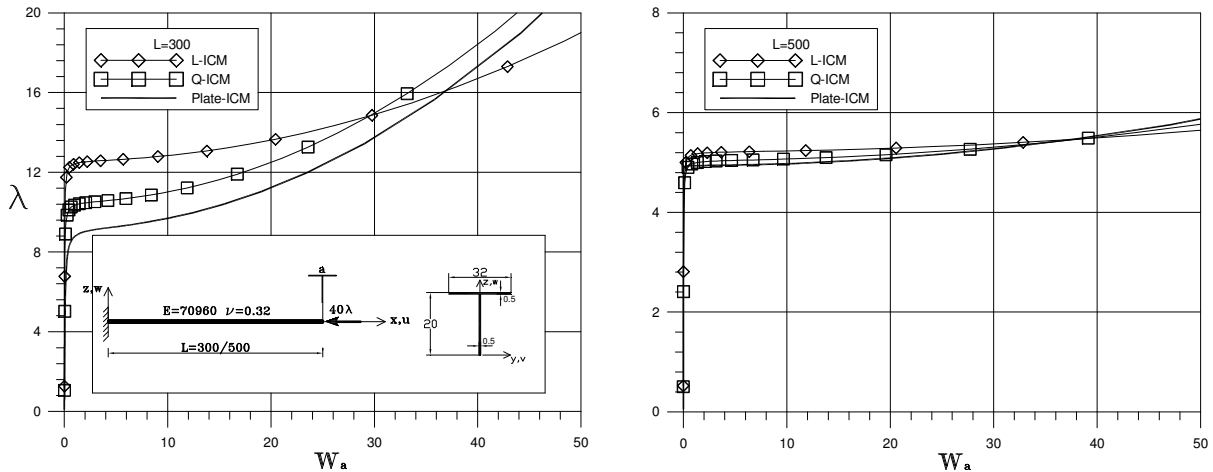


Figure 18. T-beam cantilever: equilibrium paths.

	L	L-ICM	Q-ICM	Plate
$\lambda_b$	300	12.601	10.540	9.246
	400	7.754	7.214	6.849
	500	5.219	5.049	4.940
$\ddot{\lambda}_b/2\lambda_b 10^3$	300	1.299	2.447	11.31
	400	0.6354	1.210	2.048
	500	0.3385	0.5648	0.5148

**Table 5.** T-beam cantilever: buckling parameters.

of the section, neglected in the Saint-Venant solution. The relative error rapidly reduces as the beam length increases, which confirms these interpretations.

**6.3.4. A comment about Saint-Venant beam modeling.** The proposed one-dimensional beam model represents an essential and very simple model in comparison with the plate model. It also allows a very accurate recovery of the buckling and postbuckling behavior in all cases where Saint-Venant assumptions, which are the basis of the model, are satisfied. We have, however, seen that even minor deviations from the Saint-Venant solution can have a nonnegligible effect on both the buckling and postbuckling recovery. So, there is a cost for that simplification.

The relative error could be explained by reference to three possible effects: first, the in-plane distortion of the section, which is allowed by the plate model and ignored by the beam model; second, the Vlasov increment in torsional stiffness due to nonuniform torsion, which is obliged by the Saint-Venant solution; and third, the unsatisfactory correspondence in boundary constraints between the two models which requires a different average alignment of the clamped section. The latter seems to play a major role in some of the examined test cases.

It is worth mentioning that a more accurate recovery could be obtained by refined one-dimensional models which can be derived through the ICM procedure from more sophisticated linear beam theories, such as that of [Vlasov 1959] or even better the ones obtained by the so-called GBT approach (see [Goncalves et al. 2009]) which allow a more realistic modeling of boundary conditions. An investigation of this would be of interest, but is outside the scope of the present paper. Note also that, in any case, when

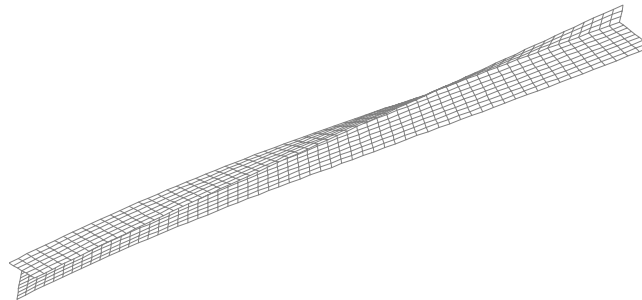


**Figure 19.** T-beam cantilever ( $L = 500$ ): buckling mode.

analyzing beam assemblages, great care has to be paid to detailed modeling of both boundary constraints and interelement connections.

**6.4. Modal interaction test: Channel beam in compression.** The inadequacy of the beam modeling becomes apparent in the presence of local buckling phenomena which produce significant in-plane section distortions, as in the case of the thin-walled Channel beam shown in Figure 20. The beam is subjected to compressive loads applied at the ends (through a uniform distribution on the sections) and to a small transversal load in the middle section (through a uniform distribution on the flanges). A simple support is also assumed at the ends of the bottom plate, and the analysis was performed by either the beam or plate assemblage models, using an eight ICM beam element mesh or  $(4 + 8 + 4) \times 45$  ICM plate elements, respectively.

The results obtained by the two models are completely different. Beam analysis recovers a simple Eulerian flexural buckling at  $\lambda_b = 1290$  (see Figure 21) and provides a stable postbuckling behavior (see Figure 23), while plate assemblage analysis further detects three distortional modes, occurring at  $\lambda_b = 1387$ ,  $\lambda_b = 1979$ , and  $\lambda_b = 2063$  (see Figure 22), and reproduces a complex coupled-buckling phenomenon characterized by a strongly unstable behavior. Note, from Figures 23 and 24, that the interaction between the first two modes changes the postbuckling making it unstable, and a secondary bifurcation, which redirects the path to a strongly unstable branch, is produced because of the activation of localized distortions due to the interaction with the other two modes.

The contribution of fourth mode is actually very small and including further buckling modes in the analysis does not change the overall behavior. This is also confirmed by an independent path-following analysis, whose results are also shown in Figure 23. Note the very good agreement between the path-following and asymptotic analysis. The two paths are practically coincident and only tend to deviate,

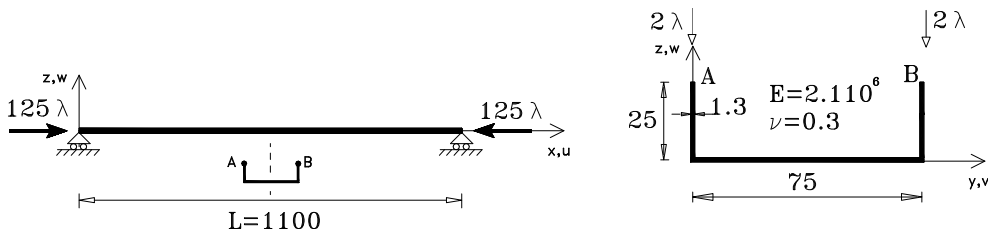


Figure 20. Channel beam: geometry.

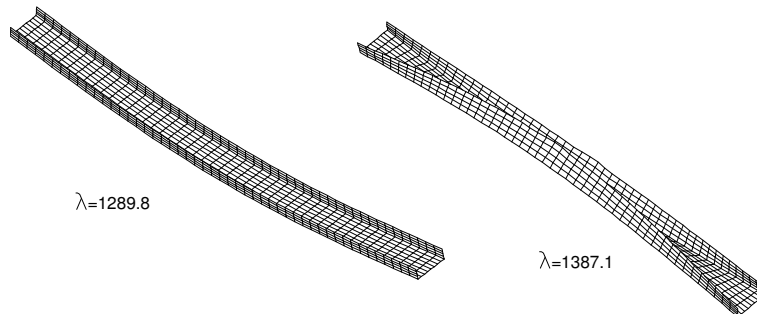
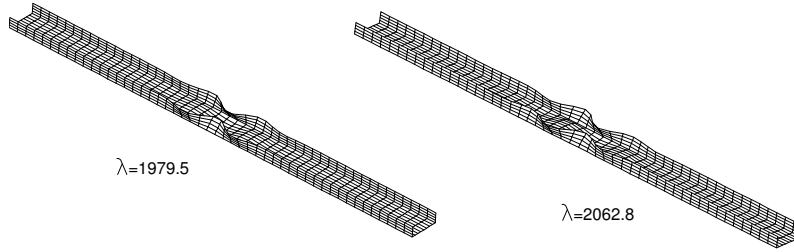
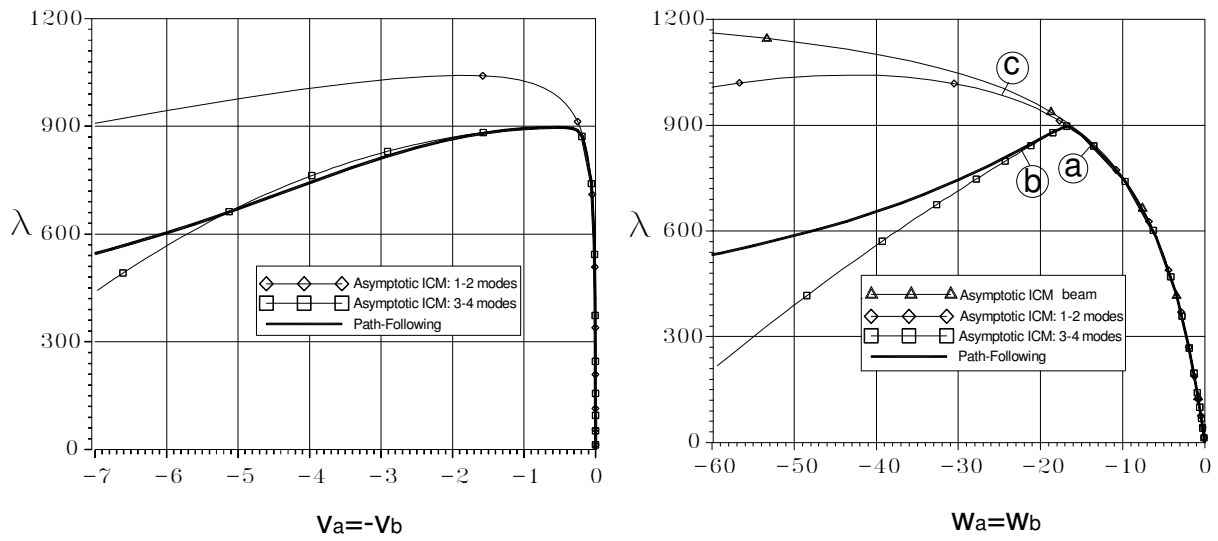


Figure 21. Channel beam: flexural and distortional buckling modes.



**Figure 22.** Channel beam: local distortional buckling modes.



**Figure 23.** Channel beam: equilibrium paths.

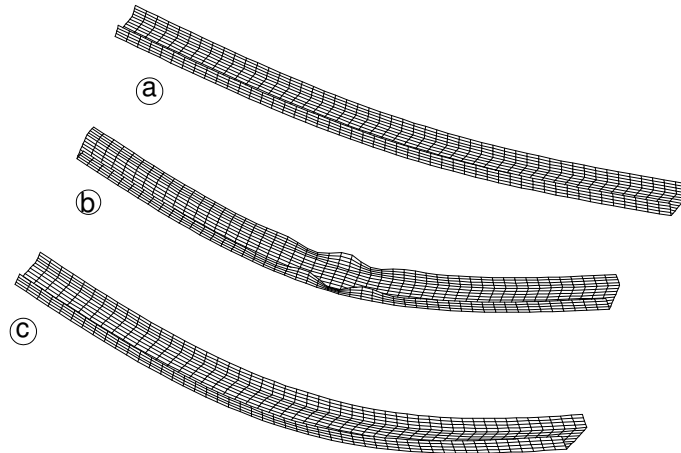


**Figure 24.** Channel beam: equilibrium configurations at a, b, and c.

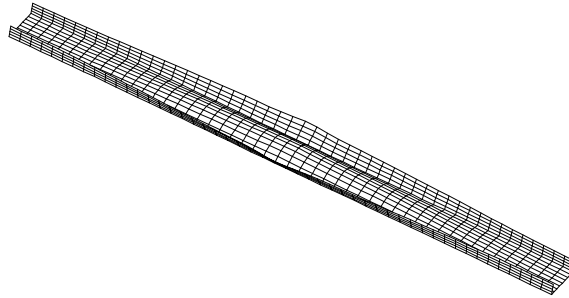


**Figure 25.** Channel beam: corrective mode in the one-mode analysis.

after the secondary bifurcation, in correspondence to a quite large distortion of the middle section (see Figure 24b). Note also that, in plate analysis, the same unstable behavior determined by the two-mode analysis is also recovered by considering the first (purely flexural) mode alone. This result might be surprising but it is due to the fact that a section distortion, similar to that coming from the second buckling mode, is also contained in the corrective mode  $w_{11}$  (see Figure 25). So the one-mode analysis can actually reproduce the flexural/distortional evolution of the buckling process.

The previous results clearly show that beam modeling, at least if based on Saint-Venant theory, can be inadequate in problems presenting coupled buckling with relevant in-plane section distortions. So it has to be used with certain care in the analysis of thin-walled folded plates. But they also show, from the results of plate analysis, the accuracy and reliability of the ICM approach in these quite difficult contexts.

## 7. Concluding remarks

The implicit corotational method (ICM) has been developed in [Garcea et al. 2012] as a general procedure for deriving frame-independent nonlinear structural models starting from the corresponding linear theories. Its use as a numerical tool, able to provide relevant results in technical practice, requires the implementation of the recovered models within a finite element approach. While the implementation procedure could be similarly as straightforward as that used in linear analysis, some difficulties can arise due to the presence of finite three-dimensional rotations and the need to assure frame invariance, as well as in the interpolation of the mechanical quantities internal to the element.

Different aspects of FEM implementation have been discussed, in relation to path-following or asymptotic analysis approaches, and some suitable strategies have been suggested to avoid locking problems related to the loss of frame invariance in the element definition or to an inappropriate format in their representation.

Two elements have been described in detail. The elements are derived from nonlinear models defined in [Garcea et al. 2012], through a separate (mixed) interpolation of the displacement and stress fields, and they are described in a mixed format which uses both stress and displacement control variables. The first element derives from the nonlinear three-dimensional beam model based on Saint-Venant rod theory described in [Garcea et al. 2012, §5]. It uses quite simple interpolation laws, directly derived from the linear case, and can be considered the simplest choice in the nonlinear beam context. The second is derived from the thin-plate model based on Kirchhoff linear theory described in [Garcea et al. 2012, §6]. It uses a spline interpolation for the translations which allows a rotation-free kinematical

description. This interpolation, which has already been used in [Garcea 2001], implies  $C^1$  continuity for the displacement field and is highly suitable for the discrete modeling of rectangular plates and their three-dimensional assemblages.

The elements have been inserted into the two computer codes COBE [Madeo 2008] and KASP [Garcea 2001], aimed at the FEM analysis of three-dimensional beam or plate assemblages, using either path-following or asymptotic solution strategies. Extensive numerical testing has been performed with these codes and some of the results have been reported and discussed in Section 6. In all cases the proposed elements show strong robustness and high accuracy when compared with existing reference analytical solutions. The good agreement between the results obtained by an independent modeling of thin-walled structures, such as Saint-Venant beams or Kirchhoff plates assemblages, gives a further mutual validation of both models, and differences, if present, are clearly related to some inadequacies in Saint-Venant linear theory. The inadequacy of Saint-Venant beam modeling in the presence of relevant in-plane section distortions, as well as the overall effectiveness of the proposed approach and its ability to recover even complex buckling behavior, is apparent from the results reported in Section 6.4.

It is worth mentioning that both proposed elements should be viewed as first simple implementation examples, only aimed at showing the effectiveness of the ICM as a computational tool to be used in FEM analysis for solving practical problems. More refined elements with even better behavior can be derived for both beams and plates, starting from the nonlinear models presented in [Garcea et al. 2012]. Further elements can also be obtained by more refined nonlinear continua which can be derived through the ICM approach as nonlinear generalizations of more sophisticated linear theories, such as, for instance, the Vlasov or GBT beam theories or laminated shell theory.

## References

- [Alsafadie et al. 2010] R. Alsafadie, M. Hjiij, and J.-M. Battini, “Corotational mixed finite element formulation for thin-walled beams with generic cross-section”, *Comput. Methods Appl. Mech. Eng.* **199**:49-52 (2010), 3197–3212.
- [Alsafadie et al. 2011] R. Alsafadie, J.-M. Battini, H. Somja, and M. Hjiij, “Local formulation for elasto-plastic corotational thin-walled beams based on higher-order curvature terms”, *Finite Elem. Anal. Des.* **47**:2 (2011), 119–128.
- [Argyris et al. 1979] J. H. Argyris, H. Balmer, S. S. Doltsinis, P. C. Dunne, M. Haase, M. Kleiber, G. A. Malejannakis, H. P. Mlejnek, M. Muller, and D. W. Scharpf, “Finite element method - The natural approach”, *Comput. Methods Appl. Mech. Eng.* **17-18**:1 (1979), 1–106.
- [Aristodemo 1985] M. Aristodemo, “A high-continuity finite element model for two-dimensional elastic problem”, *Comput. Struct.* **21**:5 (1985), 987–993.
- [Babuška 1971] I. Babuška, “Error-bounds for finite element method”, *Numer. Math.* **16**:4 (1971), 322–333.
- [Bazant and L. 1991] Z. P. Bazant and C. L., *Stability of Structures*, Dover, New York, 1991.
- [Bilotta et al. 2012] A. Bilotta, L. Leonetti, and G. Garcea, “An algorithm for incremental elastoplastic analysis using equality constrained sequential quadratic programming”, *Comput. Struct.* **102-103** (2012), 97–107.
- [Bouty et al. 2004] E. H. Bouty, H. Zahrouni, M. Potier-Ferry, and M. Boudi, “Asymptotic-numerical method for buckling analysis of shell structures with large rotations”, *J. Comput. Appl. Math.* **168**:1-2 (2004), 77–85.
- [Brezzi 1974] F. Brezzi, “On the existence, uniqueness and approximation of saddle-point problems arising from Lagrangian multipliers”, *Rev. Française Automat. Informat. Recherche Opérationnelle Sér. Rouge* **8**:R-2 (1974), 129–151.
- [Brezzi et al. 1986] F. Brezzi, M. Cornalba, and A. Di Carlo, “How to get around a simple quadratic fold”, *Numer. Math.* **48**:4 (1986), 417–427.
- [Budiansky 1974] B. Budiansky, *Theory of buckling and post-buckling of elastic structures*, Advances in Applied Mechanics **14**, Academic Press, New York, 1974.

- [Casciaro 2004] R. Casciaro, “A fast iterative solver for nonlinear eigenvalue problem”, report 35, LABMEC, University of Calabria, 2004, Available at [www.labmec.unical.it/pubblicazioni/collana.php](http://www.labmec.unical.it/pubblicazioni/collana.php).
- [Casciaro 2005] R. Casciaro, *Computational asymptotic post-buckling analysis of slender elastic structures*, CISM Courses and Lectures **470**, Springer, Wien, 2005.
- [Casciaro and Garcea 2002] R. Casciaro and G. Garcea, “An iterative method for shakedown analysis”, *Comput. Methods Appl. Mech. Eng.* **191**:49-50 (2002), 5761–5792.
- [Casciaro and Mancusi 2006] R. Casciaro and G. Mancusi, “Imperfection sensitivity due to coupled local instability: a non-convex QP solution algorithm”, *Int. J. Numer. Methods Eng.* **67**:6 (2006), 815–840.
- [Casciaro et al. 1992] R. Casciaro, G. Salerno, and A. D. Lanzo, “Finite element asymptotic analysis of slender elastic structures: a simple approach”, *Int. J. Numer. Methods Eng.* **35**:7 (1992), 1397–1426.
- [Casciaro et al. 1998] R. Casciaro, G. Garcea, G. Attanasio, and F. Giordano, “Perturbation approach to elastic post-buckling analysis”, *Comput. Struct.* **66**:5 (1998), 585–595.
- [Chen and Virgin 2006] H. Chen and L. N. Virgin, “Finite element analysis of post-buckling dynamics in plates, I: An asymptotic approach”, *Int. J. Solids Struct.* **43**:13 (2006), 3983–4007.
- [Chen et al. 2006] H. H. Chen, W. Y. Lin, and K. M. Hsiao, “Co-rotational finite element formulation for thin-walled beams with generic open section”, *Comput. Methods Appl. Mech. Eng.* **195**:19-22 (2006), 2334–2370.
- [Flores and Godoy 1992] F. G. Flores and L. A. Godoy, “Elastic postbuckling analysis via finite element and perturbation techniques, I: Formulation”, *Int. J. Numer. Methods Eng.* **33**:9 (1992), 1775–1794.
- [Garcea 2001] G. Garcea, “Mixed formulation in Koiter analysis of thin-walled beam”, *Comput. Methods Appl. Mech. Eng.* **190**:26-27 (2001), 3369–3399.
- [Garcea and Leonetti 2011] G. Garcea and L. Leonetti, “A unified mathematical programming formulation of strain driven and interior point algorithms for shakedown and limit analysis”, *Int. J. Numer. Methods Eng.* **88**:11 (2011), 1085–1111.
- [Garcea et al. 1998] G. Garcea, G. A. Trunfio, and R. Casciaro, “Mixed formulation and locking in path-following nonlinear analysis”, *Comput. Methods Appl. Mech. Eng.* **165**:1-4 (1998), 247–272.
- [Garcea et al. 1999] G. Garcea, G. Salerno, and R. Casciaro, “Extrapolation locking and its sanitization in Koiter asymptotic analysis”, *Comput. Methods Appl. Mech. Eng.* **180**:1-2 (1999), 137–167.
- [Garcea et al. 2002] G. Garcea, G. A. Trunfio, and R. Casciaro, “Path-following analysis of thin-walled structures and comparison with asymptotic post-critical solutions”, *Int. J. Numer. Methods Eng.* **55**:1 (2002), 73–100.
- [Garcea et al. 2005] G. Garcea, G. Formica, and R. Casciaro, “A numerical analysis of infinitesimal mechanisms”, *Int. J. Numer. Methods Eng.* **62**:8 (2005), 979–1012.
- [Garcea et al. 2009] G. Garcea, A. Madeo, G. Zagari, and R. Casciaro, “Asymptotic post-buckling FEM analysis using a corotational formulation”, *Int. J. Solids Struct.* **46**:2 (2009), 523–532.
- [Garcea et al. 2012] G. Garcea, A. Madeo, and R. Casciaro, “The implicit corotational method and its use in the derivation of nonlinear structural models for beams and plates”, *J. Mech. Mater. Struct.* **7**:6 (2012), 509–538.
- [Goncalves et al. 2009] R. Goncalves, P. B. Dinis, and D. Camotim, “GBT formulation to analyse the first-order and buckling behaviour of thin-walled members with arbitrary cross-sections”, *Thin-Walled Struct.* **47**:5 (2009), 583–600.
- [Hibbitt et al. 2007] Hibbitt, Karlsson, and Sorenson, “ABAQUS Version 6.7”, Pawtucket, 2007.
- [Hughes et al. 2005] T. J. R. Hughes, J. A. Cottrell, and Y. Bazilevs, “Isogeometric analysis: CAD, finite elements, NURBS, exact geometry and mesh refinement”, *Comput. Methods Appl. Mech. Eng.* **194**:39-41 (2005), 4135–4195.
- [Koiter 1945] W. T. Koiter, *On the stability of elastic equilibrium*, Ph.D. thesis, 1945.
- [Lacarbonara and Paolone 2007] W. Lacarbonara and A. Paolone, “On solution strategies to Saint-Venant problem”, *J. Comput. Appl. Math.* **206**:1 (2007), 473–497.
- [Lanzo and Garcea 1996] A. D. Lanzo and G. Garcea, “Koiter analysis of thin-walled structures by a finite element approach”, *Int. J. Numer. Methods Eng.* **39**:17 (1996), 3007–3031.
- [Lanzo et al. 1995] A. D. Lanzo, G. Garcea, and R. Casciaro, “Koiter post-buckling analysis of elastic plates”, *Int. J. Numer. Methods Eng.* **38**:14 (1995), 2325–2345.

- [M. and C. 2002] B. J. M. and P. C., “Co-rotational beam elements with warping effects in instability problems”, *Comput. Methods Appl. Mech. Eng.* **191**:17-18 (2002), 1755–1789.
- [Madeo 2008] A. Madeo, *The implicit corotational method: General theory and FEM implementation*, Ph.D. thesis, LABMEC, University of Calabria, 2008, Available at [www.labmec.unical.it/dottorato/tesi/Madeo.pdf](http://www.labmec.unical.it/dottorato/tesi/Madeo.pdf).
- [Pacoste and Eriksson 1995] C. Pacoste and A. Eriksson, “Element behavior in post-critical plane frame analysis”, *Comput. Methods Appl. Mech. Eng.* **125**:1-4 (1995), 319–343.
- [Petrolo and Casciaro 2004] A. S. Petrolo and R. Casciaro, “3D beam element based on Saint Venant’s rod theory”, *Comput. Struct.* **82**:29-30 (2004), 2471–2481.
- [Poulsen and Damkilde 1998] P. N. Poulsen and L. Damkilde, “Direct determination of asymptotic structural postbuckling behaviour by the finite element method”, *Int. J. Numer. Methods Eng.* **42**:4 (1998), 685–702.
- [Rahman and Jansen 2010] T. Rahman and E. L. Jansen, “Finite element based coupled mode initial post-buckling analysis of a composite cylindrical shell”, *Thin-Walled Struct.* **48**:1 (2010), 25–32.
- [Rankin and Nour-Omid 1988] C. C. Rankin and B. Nour-Omid, “The use of projectors to improve finite element performance”, *Comput. Struct.* **30**:1-2 (1988), 257–267.
- [Riks 1979] E. Riks, “An incremental approach to the solution of snapping and buckling problems”, *Int. J. Solids Struct.* **15**:7 (1979), 529–551.
- [Riks 1987] E. Riks, “Progress in collapse analysis”, *J. Pressure Vessel Technol. (ASME)* **109**:1 (1987), 33–41.
- [Riks 2004] E. Riks, “Buckling”, pp. xii+830 in *Encyclopedia of computational mechanics*, vol. 2, edited by E. Stein et al., Wiley, Chichester, 2004.
- [Ritto-Corrêa and Camotim 2002] M. Ritto-Corrêa and D. Camotim, “On the differentiation of the Rodrigues formula and its significance for the vector-like parameterization of Reissner-Simo beam theory”, *Int. J. Numer. Methods Eng.* **55**:9 (2002), 1005–1032.
- [Rodrigues 1840] O. Rodrigues, “Des lois géométriques qui régissent les déplacements d’un système solide dans l’espace”, *J. Math. Pures Appl.* **5** (1840), 380–440.
- [Salerno and Casciaro 1997] G. Salerno and R. Casciaro, “Mode jumping and attractive paths in multimode elastic buckling”, *Int. J. Numer. Methods Eng.* **40**:5 (1997), 833–861.
- [Salerno and Lanzo 1997] G. Salerno and A. D. Lanzo, “A nonlinear beam finite element for the post-buckling analysis of plane frame by Koiter’s perturbation approach”, *Comput. Methods Appl. Mech. Eng.* **146**:3-4 (1997), 325–349.
- [Salerno and Uva 2006] G. Salerno and G. Uva, “Ho’s theorem in global-local mode interaction of pin-jointed bar structures”, *Int. J. Non-Linear Mech.* **41**:3 (2006), 359–376.
- [Schafer and Graham-Brady 2006] B. W. Schafer and L. Graham-Brady, “Stochastic post-buckling of frames using Koiter methods”, *Int. J. Struct. Stab. Dynamics* **6**:3 (2006), 333–358.
- [Silvestre and Camoti 2005] N. Silvestre and D. Camoti, “Asymptotic-Numerical Method to Analyze the Postbuckling Behavior, Imperfection-Sensitivity, and Mode Interaction in Frames”, *J. Eng. Mech. (ASCE)* **131**:6 (2005), 617–632.
- [Vlasov 1959] V. Z. Vlasov, *Тонкостенные упругие стержни*, Fizmatgiz, Moscow, 1959. Translated as *Thin walled elastic beams*, NSF (Washington, DC) and Israel Program for Scientific Translations (Jerusalem), 1961.
- [Wu and Wang 1997] B. Wu and Z. Wang, “A perturbation method for the determination of the buckling strength of imperfection-sensitive structures”, *Comput. Methods Appl. Mech. Eng.* **145**:3-4 (1997), 203–215.

Received 30 May 2012. Revised 30 Aug 2012. Accepted 14 Sep 2012.

GIOVANNI GARCEA: [giovanni.garcea@unical.it](mailto:giovanni.garcea@unical.it)

*Dipartimento di Modellistica per l’ingegneria, Università della Calabria, Via P. Bucci Cubo 39/C 87036 Rende (CS), Italy*

ANTONIO MADEO: [antonio.madeo81@unical.it](mailto:antonio.madeo81@unical.it)

*Dipartimento di Modellistica per l’ingegneria, Università della Calabria, Via P. Bucci Cubo 39/C 87036 Rende (CS), Italy*

RAFFAELE CASCIARO: [raffaele.casciaro@unical.it](mailto:raffaele.casciaro@unical.it)

*Dipartimento di Modellistica per l’ingegneria, Università della Calabria, Via P. Bucci Cubo 39/C 87036 Rende (CS), Italy*

# JOURNAL OF MECHANICS OF MATERIALS AND STRUCTURES

jomms.net

Founded by Charles R. Steele and Marie-Louise Steele

## EDITORS

CHARLES R. STEELE Stanford University, USA  
DAVIDE BIGONI University of Trento, Italy  
IWONA JASIUK University of Illinois at Urbana-Champaign, USA  
YASUhide SHINDO Tohoku University, Japan

## EDITORIAL BOARD

H. D. BUI École Polytechnique, France  
J. P. CARTER University of Sydney, Australia  
R. M. CHRISTENSEN Stanford University, USA  
G. M. L. GLADWELL University of Waterloo, Canada  
D. H. HODGES Georgia Institute of Technology, USA  
J. HUTCHINSON Harvard University, USA  
C. HWU National Cheng Kung University, Taiwan  
B. L. KARIHALOO University of Wales, UK  
Y. Y. KIM Seoul National University, Republic of Korea  
Z. MROZ Academy of Science, Poland  
D. PAMPLONA Universidade Católica do Rio de Janeiro, Brazil  
M. B. RUBIN Technion, Haifa, Israel  
A. N. SHUPIKOV Ukrainian Academy of Sciences, Ukraine  
T. TARNAI University Budapest, Hungary  
F. Y. M. WAN University of California, Irvine, USA  
P. WRIGGERS Universität Hannover, Germany  
W. YANG Tsinghua University, China  
F. ZIEGLER Technische Universität Wien, Austria

**PRODUCTION** contact@msp.org

SILVIO LEVY Scientific Editor

Cover design: Alex Scorpan

Cover photo: Ev Shafir

See <http://jomms.net> for submission guidelines.

JoMMS (ISSN 1559-3959) is published in 10 issues a year. The subscription price for 2012 is US \$555/year for the electronic version, and \$735/year (+\$60 shipping outside the US) for print and electronic. Subscriptions, requests for back issues, and changes of address should be sent to Mathematical Sciences Publishers, Department of Mathematics, University of California, Berkeley, CA 94720-3840.

JoMMS peer-review and production is managed by EditFLOW<sup>®</sup> from Mathematical Sciences Publishers.

PUBLISHED BY  
 **mathematical sciences publishers**  
<http://msp.org/>

A NON-PROFIT CORPORATION

Typeset in L<sup>A</sup>T<sub>E</sub>X

Copyright ©2012 by Mathematical Sciences Publishers

# Journal of Mechanics of Materials and Structures

Volume 7, No. 6

June 2012

---

- The implicit corotational method and its use in the derivation of nonlinear structural models for beams and plates**  
GIOVANNI GARCEA, ANTONIO MADEO and RAFFAELE CASCIARO 509
- Nonlinear FEM analysis for beams and plate assemblages based on the implicit corotational method**  
GIOVANNI GARCEA, ANTONIO MADEO and RAFFAELE CASCIARO 539
- Damage development in an armor alumina impacted with ductile metal spheres**  
BRETT G. COMPTON, ELEANOR A. GAMBLE, VIKRAM S. DESHPANDE and FRANK W. ZOK 575
- An asymptotic method for the prediction of the anisotropic effective elastic properties of the cortical vein: superior sagittal sinus junction embedded within a homogenized cell element**  
RANIA ABDEL RAHMAN, DANIEL GEORGE, DANIEL BAUMGARTNER, MATHIEU NIERENBERGER, YVES RÉMOND and SAÏD AHZI 593



1559-3959(2012)7:6;1-8